Available online at www.sciencedirect.com
ScienceDirect
Journal of the Mechanics and Physics of Solids
55 (2007) 306–337

JOURNAL OF THE MECHANICS AND PHYSICS OF SOLIDS

www.elsevier.com/locate/jmps

On the mechanics of mother-of-pearl: A key feature in the material hierarchical structure

F. Barthelat[a,1], H. Tang[a], P.D. Zavattieri[b], C.-M. Li, H.D. Espinosa[a,*]

[a]*Department of Mechanical Engineering, Northwestern University, Evanston IL 60208-3111, USA*
[b]*GM Research and Development Center, Warren, MI 48090-9055, USA*

Received 12 December 2005; received in revised form 5 July 2006; accepted 17 July 2006

Abstract

Mother-of-pearl, also known as nacre, is the iridescent material which forms the inner layer of seashells from gastropods and bivalves. It is mostly made of microscopic ceramic tablets densely packed and bonded together by a thin layer of biopolymer. The hierarchical microstructure of this biological material is the result of millions of years of evolution, and it is so well organized that its strength and toughness are far superior to the ceramic it is made of. In this work the structure of nacre is described over several length scales. The tablets were found to have wavy surfaces, which were observed and quantified using various experimental techniques. Tensile and shear tests performed on small samples revealed that nacre can withstand relatively large inelastic strains and exhibits strain hardening. In this article we argue that the inelastic mechanism responsible for this behavior is sliding of the tablets on one another accompanied by transverse expansion in the direction perpendicular to the tablet planes. Three dimensional representative volume elements, based on the identified nacre microstructure and incorporating cohesive elements with a constitutive response consistent with the interface material and nanoscale features were numerically analyzed. The simulations revealed that even in the absence of nanoscale hardening mechanism at the interfaces, the microscale waviness of the tablets could generate strain hardening, thereby spreading the inelastic deformation and suppressing damage localization leading to material instability. The formation of large regions of inelastic deformations around cracks and defects in nacre are believed to be an important contribution to its toughness. In addition, it was shown that the tablet junctions (vertical junctions between tablets) strengthen the microstructure but do not contribute to the overall

*Corresponding author.
E-mail addresses: francois.barthelat@mcgill.ca (F. Barthelat), espinosa@northwestern.edu (H.D. Espinosa).
[1]Present address: McGill University, Montreal.

0022-5096/$ - see front matter
doi:10.1016/j.jmps.2006.07.007

material hardening. Statistical variations within the microstructure were found to be beneficial to hardening and to the overall mechanical stability of nacre. These results provide new insights into the microstructural features that make nacre tough and damage tolerant. Based on these findings, some design guidelines for composites mimicking nacre are proposed.

Keywords: Biological material; Microstructures; Mechanical testing; Strengthening and mechanisms; Finite elements

1. Introduction

Some structural materials found in nature show remarkable mechanical properties. Mostly using components with modest mechanical performances, they can achieve surprisingly high modulus, strength or toughness as a result of their very well constructed microstructures organized over several length scales (hierarchical structures, Sarikaya and Aksay, 1995). Nacre (mother-of-pearl) is a striking example of such materials. Nacre makes the inside layer of a two layer armor system mineralized by some species from the gastropod and bivalve families in order to protect their soft tissues. It is mostly composed of microscopic aragonite tablets (95% vol.), bonded by a thin layer of organic materials (5% vol.). Aragonite is a brittle ceramic, mineralized by the shell through complex processes (Schaeffer et al., 1997). Nacre has attracted much attention over the past ten years, because the toughness and strength improvements over its constituents is remarkable (Sarikaya and Aksay, 1995). The mechanical behavior of nacre has been characterized using various methods: tension (Currey, 1977), three and four-point bending (Jackson et al., 1988; Wang et al., 2001), shear (Menig et al., 2000; Wang et al., 2001) and microindentation (Wang et al., 1995). The properties of the individual components of nacre were also probed using nanoindentation (Li et al., 2004; Bruet et al., 2005; Barthelat et al., 2006a), and molecular pullout experiments using an atomic force microscope (Smith et al., 1999). In order to connect the mechanical performance of nacre with its microstructure, various models were proposed. Shear lag models and other analytical approaches were used to characterize the transfer of stress through tablets and interfaces (Jackson et al., 1988; Kotha et al., 2001; Gao et al., 2003), and finite element models were also used to characterize the stresses within tablets and interfaces (Evans et al., 2001; Katti and Katti, 2001; Ji and Gao, 2004). Following these experiments and models, several mechanisms and features have been proposed as the agents of strengthening in nacre: microstructural design (Jackson et al., 1988), small size scale of the building blocks (Currey, 1977; Gao et al., 2003), abrupt steps on the tablets surfaces (Katti et al., 2005), nanoasperities on the tablets surface (Evans et al., 2001; Katti et al., 2004; Barthelat et al., 2006a), mineral bridges across the interfaces (Song and Bai, 2003), viscoplastic deformation of the organic material (Menig et al., 2000; Okumura and de Gennes, 2001; Ji and Gao, 2004) and nanostructured tablets (Li et al., 2004). The exact features and mechanisms responsible for the strengthening of nacre are however not properly elucidated to this day (Mayer, 2005), and no clear design guideline for the design of "artificial nacre" composites with superior properties has been established. It appears that the shearing of the interface and the sliding of the mineral tablets on one another is the main deformation mechanism (Jackson et al., 1988; Sarikaya and Aksay, 1995; Wang et al., 2001). The

combination of hard components of small size with a small amount of organic material to provide relatively large inelastic deformations seems to hold the key to this behavior. However, what provides the local hardening required for mechanical stability over large deformation is not very well understood.

The objective of the present article is to demonstrate that the waviness of the tablet is the salient microstructural feature that generates hardening and damage tolerance at the macroscale. In order to better understand the mechanisms leading to the superior properties of nacre, both experiments and simulations were conducted. The article is organized as follows: The first part discusses the architecture of nacre, starting at the macroscale down to the nanoscale, with a focus on columnar nacre from red abalone (*Haliotis Rufescens*). The second part presents and discusses results from miniaturized mechanical tests. Digital image correlation (Peters and Ranson, 1982) provided the strains in different directions, and new insights into the deformation mechanisms in nacre. The third part discusses the implementation of a large representative volume element (RVE) of the microstructure of nacre using finite elements methods. The model was used to connect the mechanical behavior of nacre with its microstructure. As opposed to simplified geometries used in the past, the present model was based on actual images of the microstructure of nacre, which provided more insights into the relationships between structures and properties. Nanoscale mechanisms associated with mineral bridges, nanoasperities and biopolymer were incorporated into a cohesive law formulation to simulate the nanoscale mechanical response of the interfaces between the tablets. Finally, the paper concludes with a summary of the findings and with a set of design guidelines applicable to novel manmade composites mimicking nacre.

2. The microstructure of nacre

Nacre is part of two-layer armor system used by seashells to protect themselves from predators and other mechanical aggressions. Note that the shell is not designed for protection against hydrostatic pressure. Gastropods shells are open structures, and bivalve shells are most often open for the purpose of feeding. The outer layer of the shell is made of large prismatic calcite grains, while the inside layer is made of nacre (Fig. 1). The calcite layer is hard and suitable to prevent penetration of the shell, but it is prone to brittle failure. Nacre is softer, can withstand larger inelastic deformations, and can dissipate significant mechanical energy. It is much tougher than the calcite layer, so even if the brittle outside layer cracks the nacreous layer can retard catastrophic failure and preserve the integrity of the shell. Such armor system (hard outside with a softer backing plate) is believed to be ideal for an armor system (Sarikaya and Aksay, 1995). In order to achieve high mechanical performances, the microstructure of nacre is very well organized over several length scales. Nacre is composed of 95% vol. of aragonite $CaCO_3$, which is organized in polygonal tablets stacked to form a brick wall like structure (Fig. 2a, b). In columnar nacre, the tablets are stacked in columns across the layers. This type of nacre can be found in *Haliotis Rufescens* (red abalone), *Trochus Niloticus* (top shell) and other gastropods (Currey and Taylor, 1974). Sheet nacre is a different type of nacre, which can be found in bivalve species such as oysters or mussels. In sheet nacre the arrangement of the tablets from one layer to the next is more random. In order to characterize the exact arrangement of the tablets in columnar nacre, a sample of nacre was harvested from a red abalone specimen. The sample was cleaved along the tablet interfaces and fluorescent dye

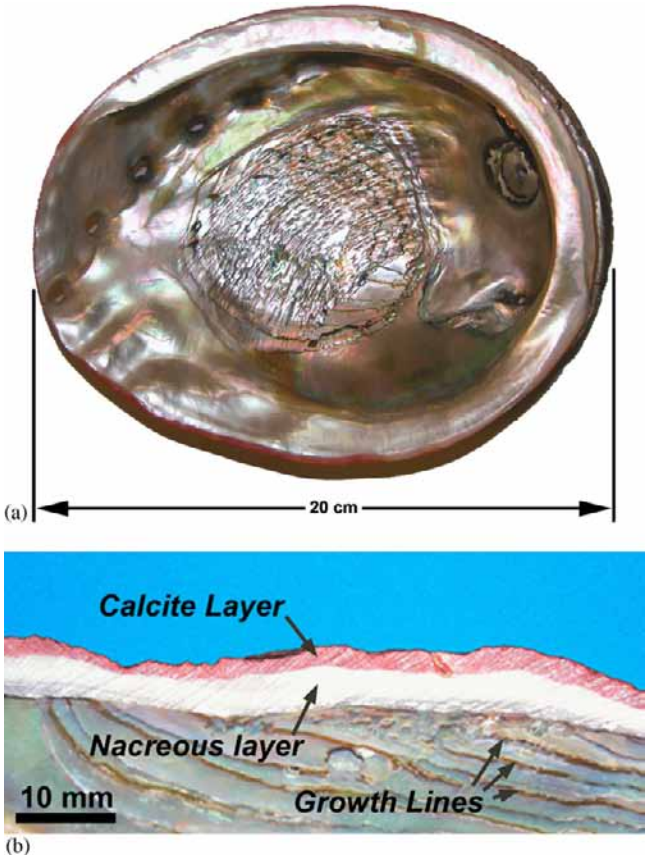

Fig. 1. (a) View of the inner nacreous layer of a red abalone shell. (b) Typical arrangement of shells using nacre.

was applied on both surfaces to highlight the tablet boundaries. Optical imaging of the cleaved surface shows a Voronoi like tiling of the tablets within one layer (Fig. 2c). The area of individual tablets was measured using image analysis, and was found to follow a normal distribution (mean = 35 μm^2, standard deviation = 10 μm^2). The opposite side of the cleaved specimen was also imaged. Using features easily recognizable on both surfaces (such as specimen corner or tablet steps), the two tablet contours were superimposed to accurately reconstruct the arrangement of the tablets from one layer to the next (Fig. 2d). The contours are consistent with tablets arranged in columns, with some overlap between tablets from adjacent columns. The pattern can therefore be divided into two regions: The "core" is the region which is common to the tablets belonging to the same column, and the "overlap" region corresponds to the areas where tablets from adjacent columns overlap (Fig. 2e). The overlap areas cover about 1/3 of the surface area of the tablet layers. The distinction between these two regions is important as they experience significantly different stress states.

The tablets in nacre are often described and modeled as flat at the microscale. Closer examination reveals that this is not the case, and that the interface between the tablets shows a prominent waviness (Fig. 3a, b). This feature was observed using (1) optical

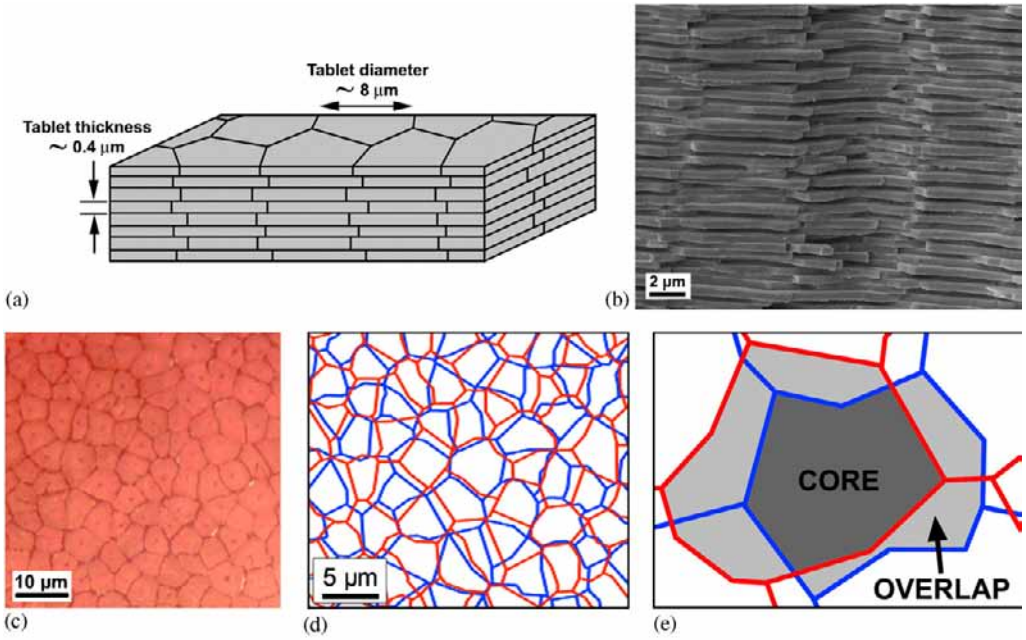

Fig. 2. Nacre at the mesoscale: (a) schematic of the tablets arrangement in nacre; (b) scanning electron micrograph of a fracture surface in nacre; (c) top view of tablet tiling in nacre; (d) reconstitution of the arrangement of the tablets from one layer to the next; (e) core and overlap areas in the tablet arrangements.

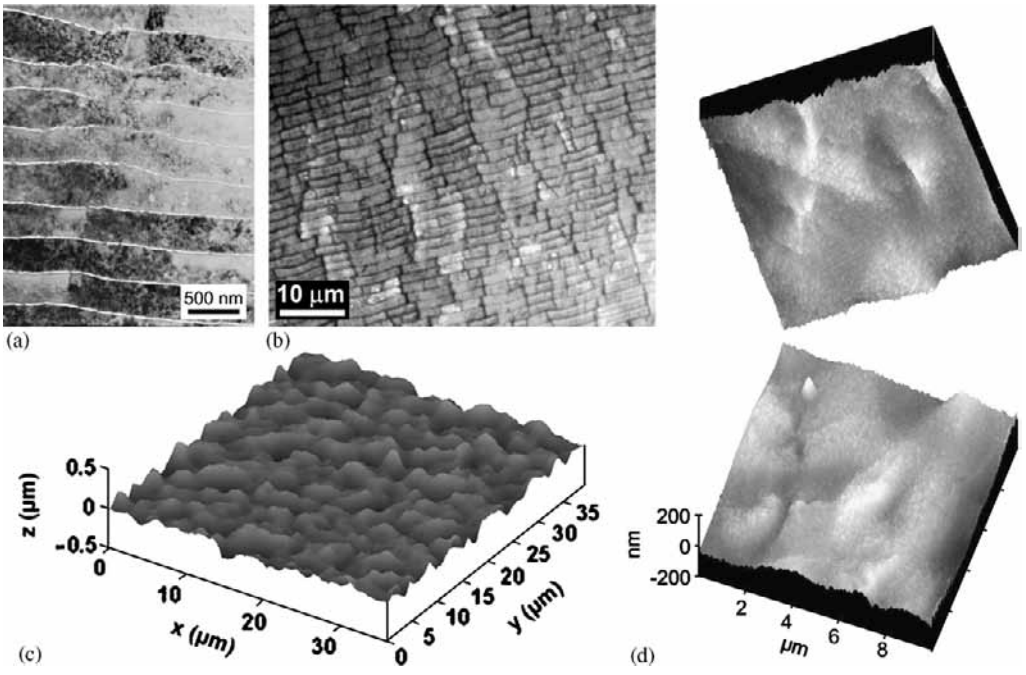

Fig. 3. Nacre at the microscale: (a) transmission electron micrograph of nacre from red abalone showing tablet waviness; (b) optical micrograph of nacre from fresh water mussel *Lampsilis Cardium;* (c) layer topology from laser profilometry; and (d) atomic force micrographs of opposed tablets, showing high degree of conformality.

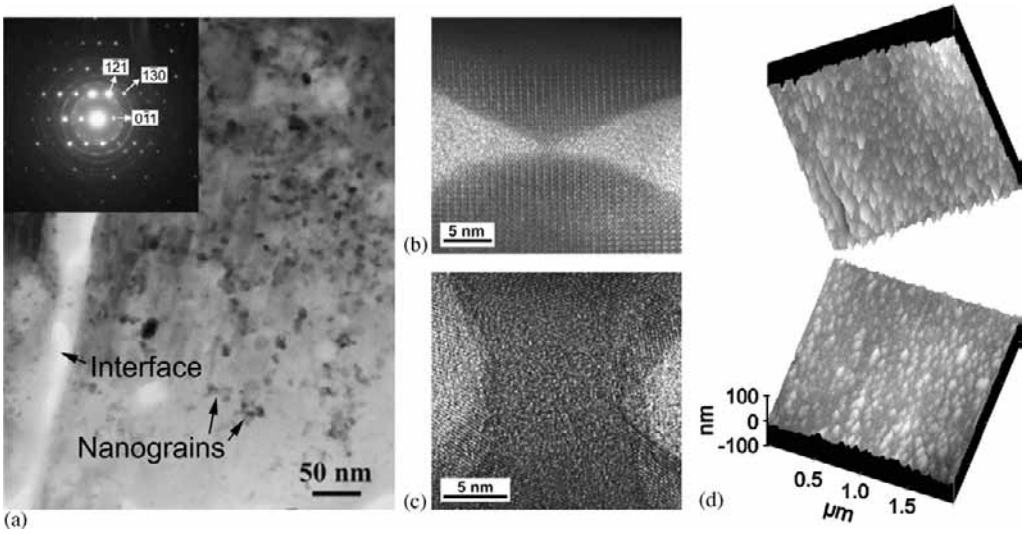

Fig. 4. Nacre at the nanoscale: (a) TEM of a nacre tablet, showing nanograins inclusions; (b) high resolution TEM of asperity inside a tablet interface; (c) high resolution TEM of an aragonite bridge connecting two tablets across the interface; and (d) AFM of opposed tablet surfaces showing nanosize features.

microscopy (2) SEM (3) TEM (4) laser profilometry and (5) atomic force microscopy (AFM). The waviness was also characterized using a laser profilometer (Fig. 3c). Roughness analysis revealed a root mean square (RMS) of 85 nm, for an average peak-to-peak distance of 3 μm. The roughness can reach amplitudes exceeding 200 nm, which is a significant fraction of the average thickness of the tablets (450 nm). AFM on the opposed faces of a cleaved sample (Fig. 3d) shows that the topology of the surface from one tablet to the next is highly conformal, so that the tablets fit perfectly together. Interestingly, the waviness of the tablets was also observed for a nacre specimen from the bivalve group (fresh water mussel *Lampsilis Cardium,* Fig. 2b) and can also be seen on nacre from many other species (Manne et al., 1994; Feng et al., 2000; Song and Bai 2002; Blank et al., 2003), although its impact on mechanical performance has never been explored. The smallest features in the architecture of nacre can be found at the nanoscale (Fig. 4). The tablets are mostly made of single aragonite grains, with the [0 0 1] crystallographic orientation normal to the plane of the tablets (Sarikaya and Aksay, 1995). Fig. 4a shows a transmission electron micrograph which reveals the presence of nanograins within the tablets. These nanograins appear as inclusions, as it is evident from concentric rings superimposed to the diffraction pattern of aragonite. Note that the concentration of nanograins appears to be much smaller than what was observed by Li et al. (2004) using AFM.

The interface between the tablets is 20–30 nm thick. It is a complex system mainly composed of biopolymer species organized into several layers (Schaeffer et al., 1997). Direct aragonite bridges and nanoasperities on the surface of the tablets are believed to provide direct mechanical interaction between tablets (Wang et al., 2001; Song and Bai, 2003). Both features were observed using high resolution TEM (Fig. 4b, c). Atomic force microscopy on a cleaved sample shows the distribution of these nanosize features on the surface of the tablets (Fig. 4d). Their density and size can vary significantly from one area

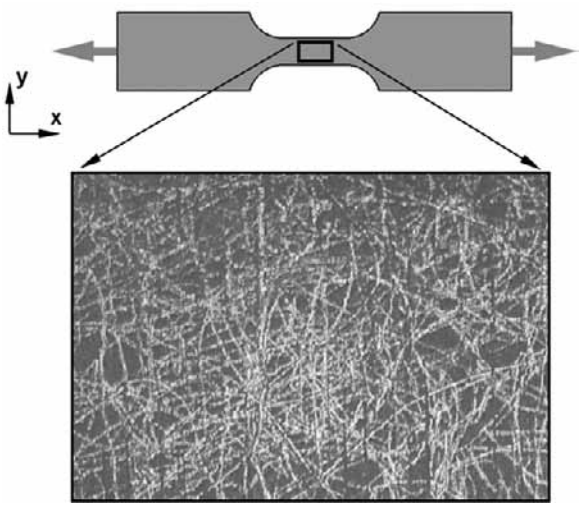

Fig. 5. Microscope field of view of the gage of the tensile specimen. The surface of the specimen surface was lightly scratched to provide the features needed for image correlation.

to another (Barthelat et al., 2006a), and in average they are 10–30 nm in size (height and width), with a spacing in the order of 100–200 nm (Fig. 5).

3. Nacre in tension

Cracking and failure resulting from tensile stresses are often the main concern for ceramics as structural materials. Ceramics exhibit very limited plasticity and are very sensitive to initial flaws, which are generally the crack starters that can lead to brittle, catastrophic failures. The structure of nacre is probably optimized for tensile strength in the direction of the tablets, as well as resistance to cracks running across the tablets (tensile strength and toughness are actually related for a material like nacre). Mechanical aggressions such as a predator's bite or the impact of a rock displaced by tidal currents impose a concentrated load normal to the surface of the shell. As described above, the outer prismatic layer is hard and prevents penetration. In this configuration, however, the shell experiences bending stresses. As a result the outer layer is subjected to compression (which is not a concern for the hard ceramic it is made of), and the inner nacreous layer is subjected to tension along the tablets. Tensile strength is therefore an important attribute for nacre and the shell as a whole. In the case of a more severe loading, cracks may propagate from the contact area throughout the prismatic layer (as cracks emanate from the corners of a Vickers indent on a ceramic surface). Once the brittle outside layer is cracked, only the stronger and tougher nacreous layer can retard catastrophic failure and preserve the integrity of the shell. From these two examples, it is clear that tensile strength and toughness are critical properties for nacre. Note that the tensile behavior of nacre and its associated mechanisms are central to most studies on this material (Currey, 1977; Jackson et al., 1988; Sarikaya and Aksay, 1995; Katti and Katti, 2001; Wang et al., 2001).

In order to assess the behavior of nacre in tension, small dog-bone shaped specimens were harvested from the nacreous layer of a red abalone shell. The width of the gage was

1.5 mm and the thickness was 0.6 mm, with a gage length of 1.5 mm, and an overall length of 20 mm. The specimens were cut such that their axis was aligned with the plane of the tablets. For the tensile test, a miniature loading stage (Ernest F. Fullam, Inc., Latham NY) equipped with a 100 lbs load cell was used. The loading stage was placed under an optical microscope, and pictures of the gage were taken at regular intervals. The pictures were used to determine the full displacement field of the sample surface, at different loading levels, using digital image correlation (Peters and Ranson, 1982). The method essentially tracks the displacements of the surface of the specimen from a reference image (unloaded specimen) to a deformed image (stretched specimen). The surface of the specimen must show dark and light features, which in this case were generated by lightly scratching the specimen surface with a needle. All the image correlations were performed using the software VIC2D (Correlated Solutions, West Columbia, SC). The specimens were loaded at a strain rate of about $0.001\,s^{-1}$, up to failure. After failure, pictures of the two broken pieces were acquired to determine the strain recovery, also by digital image correlation. Typical displacement fields from a tensile experiment are shown in Figs. 6a and b.

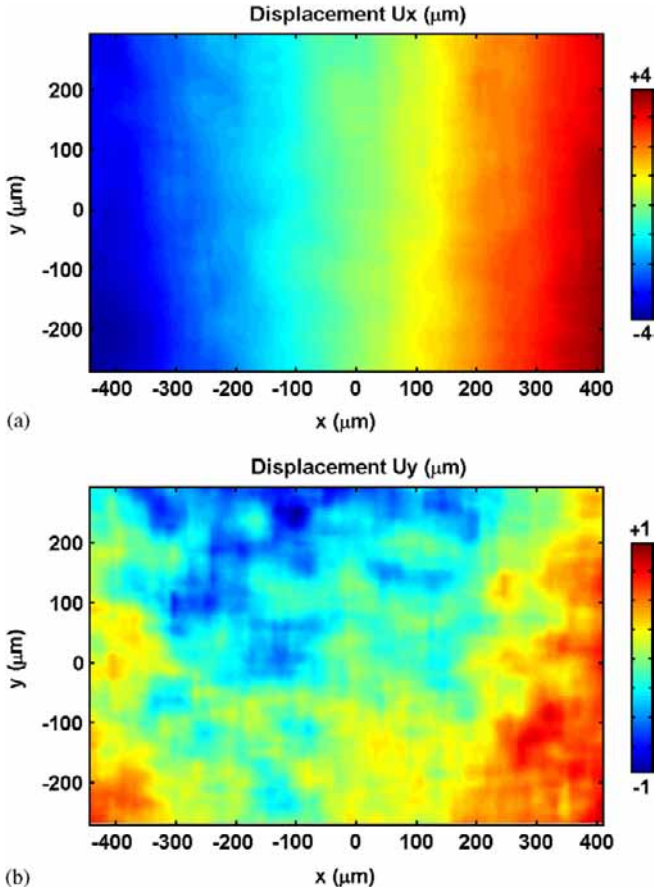

Fig. 6. Typical results from image correlation: (a) displacement field in the axial direction (stretching direction) and (b) displacement field in the transverse direction. These displacements were used to compute the average strains in the gage of specimen.

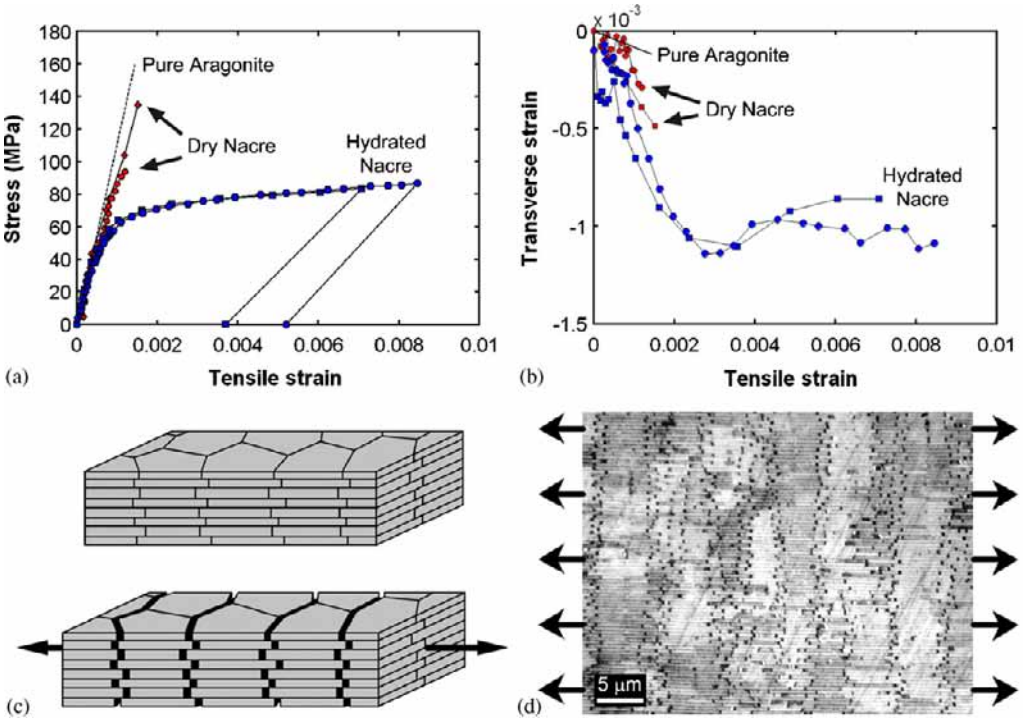

Fig. 7. (a) Stress–strain curve of nacre in tension along the tablets. (b) Transverse strain as function of longitudinal strain. (c) Schematic showing tablet sliding. The tablet separation generates voids at the end of the tablets. (d) Micrograph of a tensile specimen showing that all the potential sliding sites were activated. The dark spots are voids generated by tablet separation.

The average engineering strains in the specimen were determined from the displacement fields. Specimens were tested under both dry (ambient conditions) and hydrated conditions (soaked in water). Two specimens were tested for each case. The resulting stress–strain curves are shown in Fig. 7a. Dry nacre behaved like a monolithic ceramic and failed in a brittle fashion. The response was linear elastic (E~90 GPa) up to a failure stress of 135 MPa (specimen #1) and 95 MPa (specimen #2). The behavior of dry nacre is similar to that of pure aragonite, also plotted in Fig. 7a. By contrast, hydrated nacre showed a linear elastic response (E~70 GPa) followed by a region of larger inelastic strains starting at a stress of 70 MPa. As the strain increased the material hardened and the inelastic deformations spread throughout the specimen (Fig. 8a). The full strain field obtained from image correlation revealed a uniform strain distribution in the specimen throughout the test (Fig. 8a). Failure occured at a strain of almost 0.01 (locally, the strain could reach 0.015, Fig. 8a), which is a significant level of deformation for a material mostly made of ceramic. Once unloaded, the material recovered about 50% of the total deformation, and the modulus dropped to about 25 GPa, which is an indication of damage accumulations in the straining process. The modulus and strength from this tensile test are consistent with previous experiments using a four-point bending configuration (Wang et al., 2001).

These relatively large deformations in nacre are generated through specific mechanisms. Tensile stresses are channeled from tablet to tablet through shear stress in the overlap

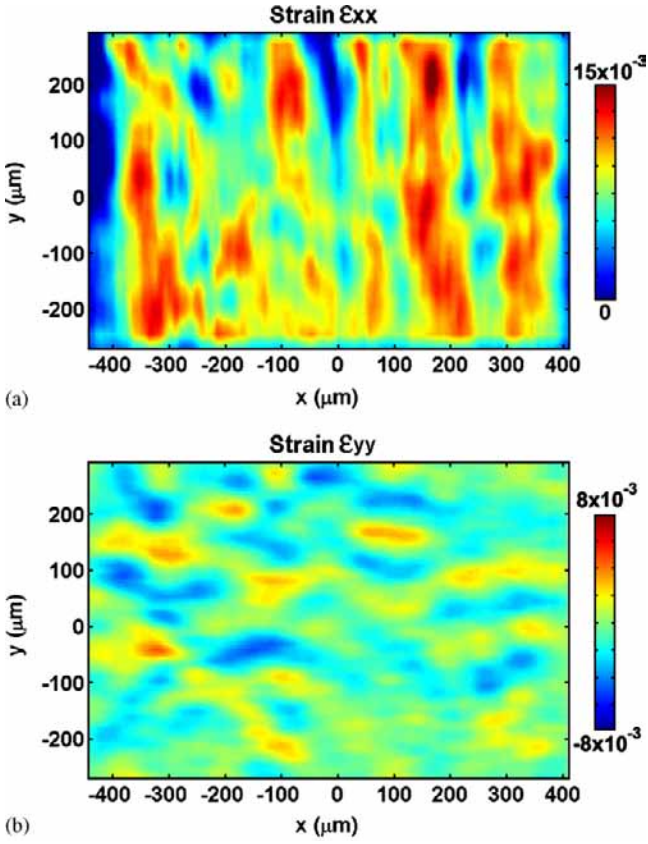

Fig. 8. Strains in the specimen immediately prior to failure: (a) longitudinal strain ε_{xx} (average is 0.084); (b) transverse strains ε_{yy} (average is -0.01).

regions. When the shear strength of the interfaces is reached, the tablets start to slide on one another and in this process; the separation of the tablets generates voids. Tablet sliding is the source of the relatively large strains observed at the macroscale. Post mortem examination shows that sliding occurs in the overlap regions and that at failure all the potential sliding sites were activated throughout the specimen (Fig. 7d). A fundamental requirement for this type of behavior is that some type of hardening mechanism must take place at the interface. As tablets start to slide, higher stresses are required to slide them further so that it is more favorable for the material to initiate new sliding sites, thus spreading deformation over large volumes.

The transverse strains in the specimen were also determined. Fig. 7b shows that initially the specimen contracted laterally, with Poisson ratios $v = 0.3$ and 0.4 under dry and hydrated conditions, respectively. Once tablet sliding was well established for the hydrated case (tensile strain >0.002), the transverse contraction ceased and a slight transverse expansion was observed. From there, the transverse strains remained constant with a value of about -0.001. No additional contraction due to Poisson's effects in the tablets was observed, because in this regime tablet sliding is the dominant mode of deformation and no

additional strains are generated within the tablets. It is possible that as the tablets slide on one another some transverse expansion is generated in the transverse direction, which would counteract the Poisson's effect. This phenomenon can be clearly seen in the shear tests that are discussed in the subsequent sections.

These results showed significant differences between the mechanical responses of hydrated and dry nacre, which can be explained by differences between dry and hydrated organic material. In order to investigate this hypothesis, the mineral tablets from a nacre sample were dissolved using a 5% solution of hydrochloric acid. Note that a similar process was used in the past to characterize the different layers of the organic material (Schaeffer et al., 1997). After dissolution in the solution the remaining organic material appeared to be soft and rubbery. However, after leaving the sample in the ambient conditions for about 2 or 3 days, the organic material had dried and had become extremely fragile and brittle. The dissolution process might introduce chemical changes and alter the organic material, but it would probably not change these basic observations: dry organic material appears to be brittle, while hydrated organic material is soft and rubbery. Dry organic interfaces therefore probably fail at small strains, and are not capable of sustaining large deformations. Hydrated interfaces, on the other hand, can deform and maintain the cohesion between the tablets over larger displacements, which is important for tablet sliding and for achieving large strains.

4. Nacre in shear

From the previous experiments and observations, it is clear that tablet sliding is the prominent source of deformation. In this mechanism the tablets are essentially linear elastic, while the inelastic behavior is provided by shearing of the interfaces (Gao et al., 2003). In order to investigate interface shearing in a more direct fashion, shear tests were performed. First, a simple shear configuration was used on small samples of nacre (1 mm × 1 mm × 1 mm, Fig. 9a). The specimens were cut and mounted on the fixture so they were sheared along the tablets layers. The setup was similar to the one used in Menig et al. (2000) but it was augmented with optical strain determination. The loading stage was placed under an optical microscope, and pictures of the gage were used to determine the strains. The specimens were loaded at an engineering shear strain rate of about $0.002\,s^{-1}$. Failure occurred along the plane of the tablets, following an interface layer. The fracture surface was mostly smooth and iridescent, with very little steps. After failure, image correlation on the broken pieces yielded the residual strains. Fig. 9b shows the resulting shear stress–strain curve. (The engineering shear strain $\gamma_{xy} = \partial u_x/\partial y + \partial u_y/\partial x$ was used to characterize the shear deformations). After an initial linear response (shear modulus = 14 GPa in dry condition, 10 GPa in hydrated condition), a region of large shear strains and hardening initiated at a shear stress of about 20 MPa, up to a failure shear strain of about 0.15. Fig. 10 shows that the strains were distributed uniformly in the gage, with no sign of localization. The stress levels in this test were much lower than the strength of the tablets (Barthelat et al., 2006a), and therefore shearing of the interface was the prominent deformation mechanism in this experiment. As the stress was increased, the layers of aragonite tablets sled on one another, creating a staircase like deformation (Wang et al., 2001) and generating large deformations. Hardening at the interface is a requirement for such behavior. Surprisingly, the dry specimen also showed significant shear deformations, although the shear stress at which yield occurs was higher (55 MPa) and

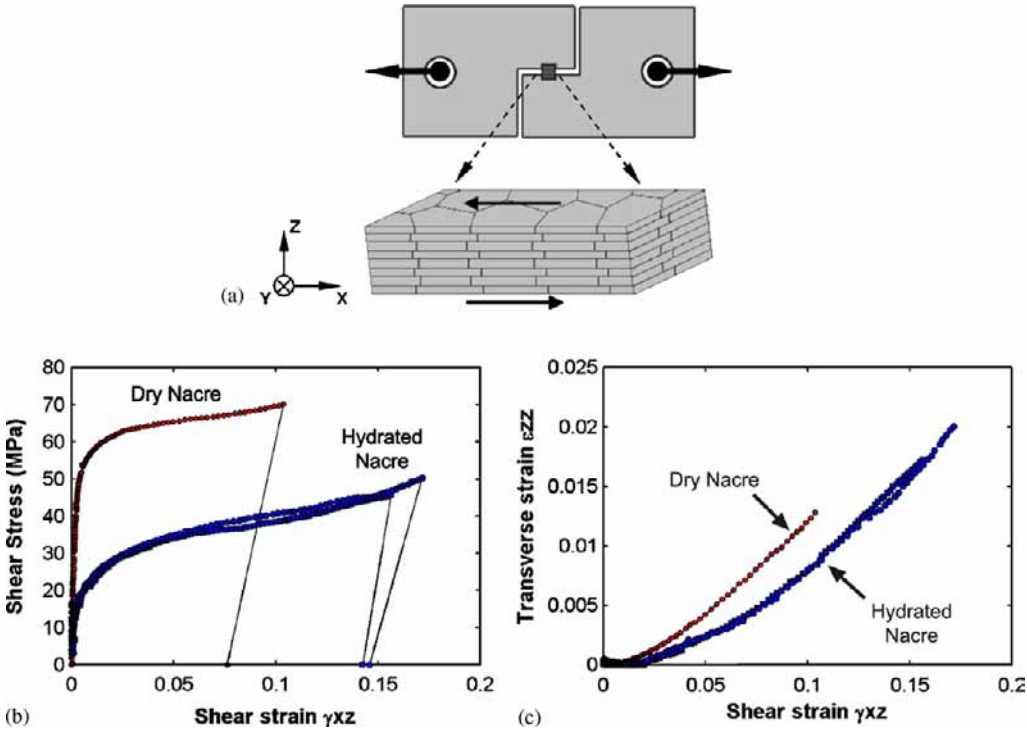

Fig. 9. (a) Simple shear setup. (b) Shear stress–strain curve in dry and hydrated conditions. (c) Transverse strain (expansion) in dry and hydrated conditions.

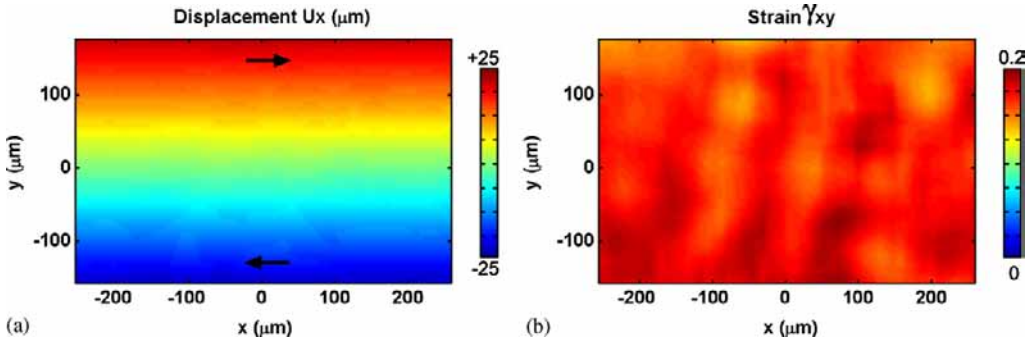

Fig. 10. Image correlation one the last image before failure in shear for hydrated nacre: (a) displacement field; and (b) engineering shear strain field.

the shear strain at failure was smaller (0.1). In comparison with the tensile configuration, it seems that the shearing configuration is more stable and produces more hardening. The interface is the source of hardening in nacre, and since the entire area of the interfaces is sheared during a shear test, a more pronounced hardening was observed. During a tensile

test the interfaces are sheared only in the overlap areas (30% of the interface area) which would explain why the hardening rate in tension was lower than in shear.

During the shear tests, the strains *across* the tablet layers were also determined from the full field displacements. For both dry and hydrated cases, shearing was accompanied by a significant expansion across the layers, up to 0.02 for the hydrated case and 0.015 for the dry case (Fig. 9c). This type of behavior, observed for the first time in nacre, clearly suggests that the layers have to climb some type of obstacles in order to slide on one another.

5. Nacre in shear-compression

The second type of shear test employed was the off axis compression. These tests were performed to investigate the effect of normal pressure on interface shearing and tablet sliding. The specimens were nacre prisms (1 mm × 1 mm section, 2 mm height) cut so that the layers oriented at about 45° from the loading axis, as in Wang et al. (2001), but again augmented with optical strain measurements (Fig. 11a). In this configuration the layers were loaded in shear and in compression with equal magnitude. The specimens were

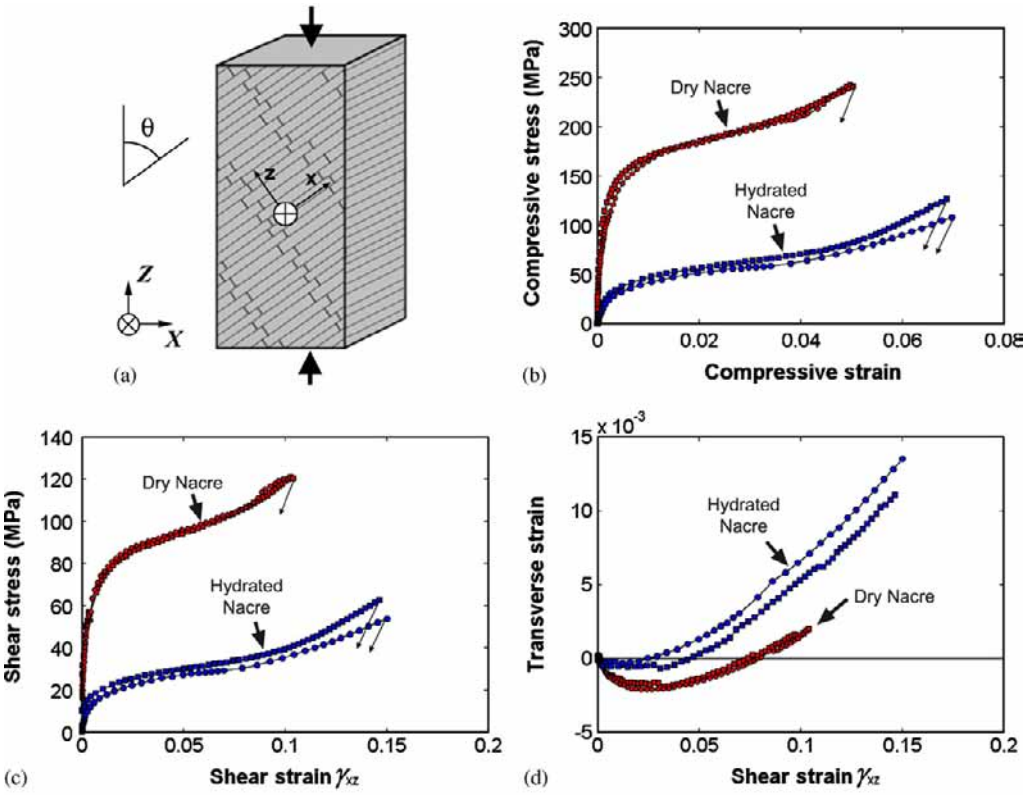

Fig. 11. (a) Off-axis specimen and loading direction. (b) Compressive stress–strain curve. (c) Shear stress–strain curve along layers after Mohr's transformation. (d) Expansion across layer.

compressed at a strain rate of about $0.001\,s^{-1}$, up to failure. Like in the simple shear experiment, the failure always occurred along an interface. Hence, the exact angle between tablet layers and loading axis could be determined by measuring the angle of the failure surface (between 46° and 48°, depending on the specimen). As in the previous experiments, the full displacement fields were determined using image correlation. Fig. 11b shows the compressive stress–strain curve in the global coordinates (X, Y, Z) as directly measured in the specimen. The off axis compression curve in hydrated condition is similar to the one obtained by Wang et al. (2001). However the present test yielded more information, with the measurement of strains in two directions on the surface of the specimen. Mohr's transformations were performed to obtain the shear stresses and strains in the local coordinate system (x, y) which is oriented along the layered structure (Fig. 11a). In this coordinate system, the interfaces are in a shear-compression state of stress. The results are shown on Fig. 11c and d. The stress–strain curves showed a significant amount of inelastic deformations before failure, with the material being again stronger in dry conditions. In the linear elastic region the compression across the layers generated compressive strains of increasing level. As the tablets started to slide, the trend was reversed and the layers expanded across the interfaces. This is additional evidence of some climbing mechanism during sliding of the layers on one another. Note that dry specimens started to yield at higher shear stresses than for the hydrated case, which also means higher compression level across the layers. This explains why the compressive stress and strains across the layers are higher for the dry case (Fig. 11c). The behaviors in simple shear and shear-compression are compared on Fig. 12. Under hydrated conditions, both configurations produced the same behavior up to a shear strain of 0.1. Beyond this point, the transverse compression appeared to increase the shearing resistance of the interface. In dry condition, the normal compression increased the overall resistance to shear, from the point where sliding begins. This suggests that over a large range of deformation the shearing resistance of the interfaces is essentially pressure independent, under the condition that nacre is hydrated. It is likely that such behavior is due to lubrication processes which would only take place in hydrated conditions (Evans et al., 2001). All tests showed that shearing of the layers was accompanied by a significant lateral expansion (Fig. 12b).

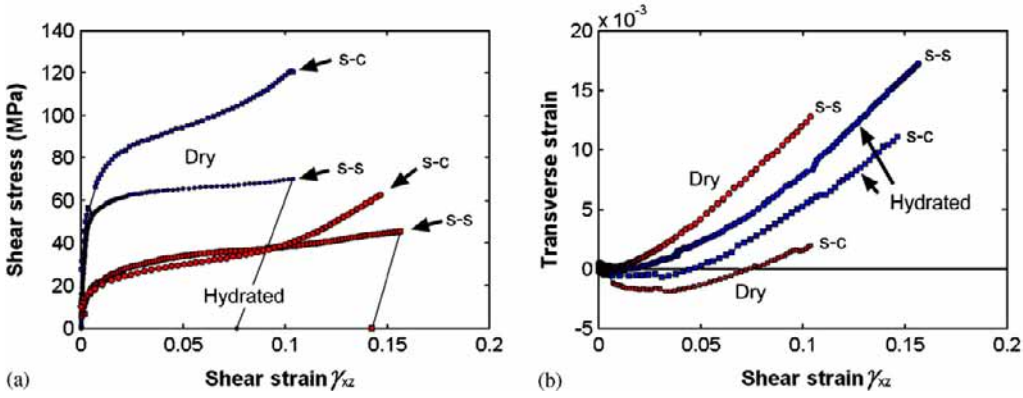

Fig. 12. Comparison of simple shear (s–s) and shear-compression (s–c) responses: (a) shear stress–strain curves; (b) transverse strain as function of shear strain.

The structural features which have the potential to generate such behavior are now examined. The biopolymer at the interface is a complex multilayered system (Schaeffer et al., 1997). Experiments by Smith et al. (1999) demonstrated that some of the molecules composing the organic interface were capable of very large extension, by sequential unfolding of the modules they contain. This process, however, operates at more or less constant stress, and these molecules did not show significant hardening over the range of stretching explored (100 nm, which is also in the order of the observed tablet sliding distances). Even if hardening in the biopolymer constitutive behavior is assumed, it is important to note that such behavior per se cannot explain the transverse expansion observed experimentally. Another source for local hardening, proposed in the literature (Song and Bai, 2003) is the existence of mineral bridges across the interfaces. In the context of tablet sliding, bridges could add to the initial shear strength of the interface. However, they would fail at relatively small strains, and as a result they could not provide the needed resistance to sliding over the distances observed experimentally. The only structural features that could act as obstacles to tablet sliding and produce transverse expansion are: (i) nanoasperities and (ii) microscale tablet waviness. The first hypothesis is now examined. To properly function as obstacles, the nanoasperities need to interact over large sliding distances in both shear and tensile configurations. The present shear test yielded a maximum shear strain of 0.015. Assuming that the tablets are rigid and that the shear deformations are concentrated in the 30 nm thick interfaces (the tablets being 450 nm thick), such strain level would correspond to a sliding distance of about 75 nm. On post mortem tensile specimens even larger sliding distances were actually observed, as tablets separation resulting from sliding could reach 100–300 nm. By comparison, the average asperity width is about 10–30 nm and therefore their interaction is limited to relatively short sliding distances. The simulation models presented by Evans et al. (2001) showed that the asperities provide increased resistance to tablet sliding up to 15–20 nm only. In addition, TEM observations revealed that the number of asperities that seem to actually be in contact across the interface is relatively small (Barthelat et al., 2006a). Nanoasperities might contribute to the initial strength of the interface. However, they are too small in size, and their interactions seem too limited to produce the observed hardening. The microscale waviness of the tablets, on the other hand, is a feature with a larger size, which could produce hardening and transverse expansion over the experimentally observed table sliding distances. If this explanation is correct, *no nanoscale hardening is required* at the interface. This mechanism is investigated in detail in the next section, using numerical simulations.

6. Finite element models

In order to demonstrate the effects of tablet waviness on the mechanical behavior of nacre, numerical simulations of a three-dimensional representative volume element (RVE) of hydrated nacre were performed using ABAQUS (Version 6.4-1, ABAQUS, inc. Providence, RI). The actual tablet contours and arrangement obtained from optical images (see Fig. 2d) served as the basis for this model. The contours were slightly modified at the edges to make the contours periodic in both x and y directions. Based on these contours, a three dimensional finite element model of two consecutive layers of tablets was built. In order to incorporate the actual statistical variations of tablet size, shape and arrangement, about 150 tablets were included in each layer. The resulting RVE was $72 \times 78\,\mu m$

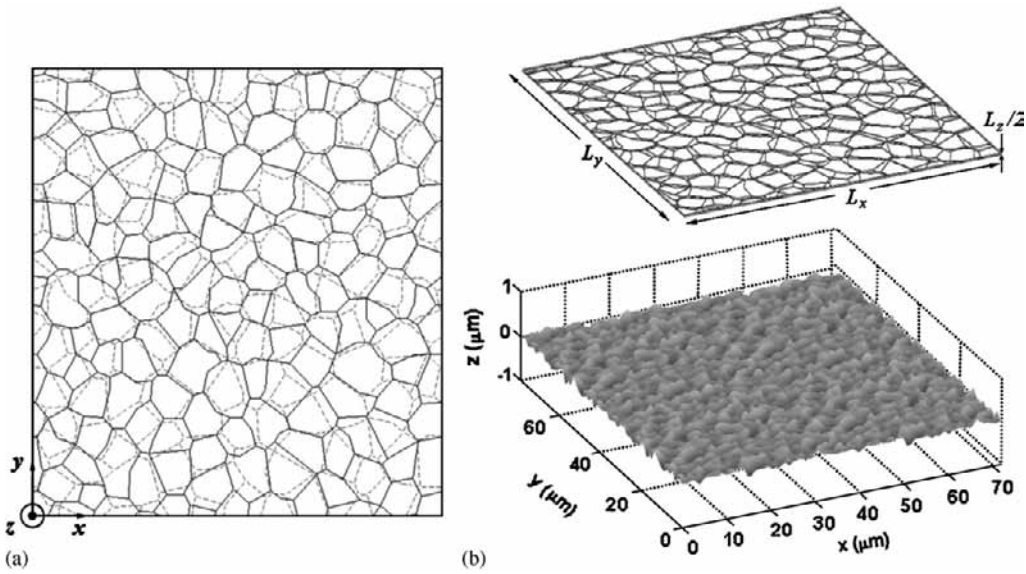

Fig. 13. (a) Tablet contours of the two layers. (b) 3D model and plot of the waviness incorporated at the interfaces.

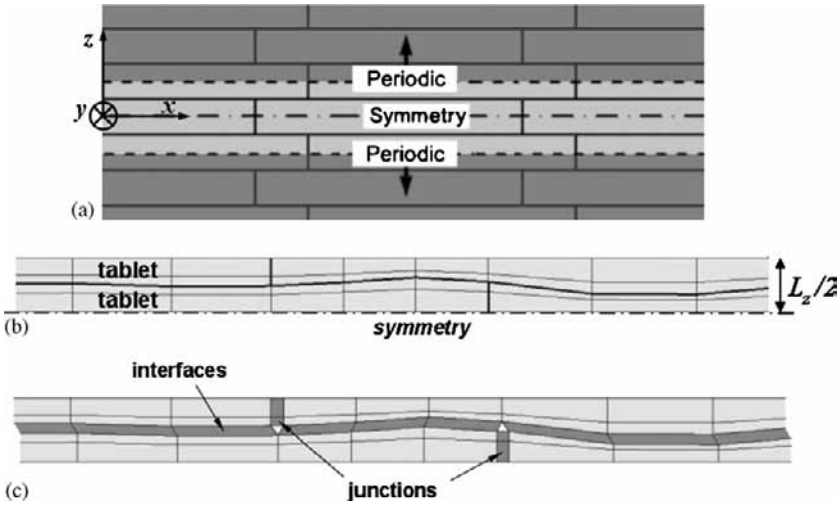

Fig. 14. (a) Schematic showing the conditions of periodic/symmetric RVE. (b) Detail of a cross section of the three-dimensional meshed model. Thicker lines show the location of cohesive elements at the interfaces and junctions. (c) Exploded view of the same cross section showing the location of the cohesive elements at the interfaces and at the junctions.

(Fig. 13a, b). In order to reduce computational cost, the RVE was assumed to be symmetric about the $x-y$ plane (Fig. 14a) so only half tablets were modeled (Fig. 14b). The boundaries between tablets were separated into two categories. The *interfaces* composed

the horizontal tablet boundary layer (normal to z), while the *junctions* were the vertical walls between the tablets. A "flat" model was generated with a perfectly flat interface, while a "wavy" model had a wavy interface, implemented using actual data from laser profilometry (Fig. 13b). The edges of the wavy surface were also slightly modified in order to make it periodic in both x and y directions. Periodic boundary conditions were imposed along all three directions, viz.

$$\begin{aligned} &u(x+L) = u(x) + \bar{\varepsilon}L, \\ &t(x+L) = -t(x) \qquad \forall x \in \text{RVE boundary}, \end{aligned}$$

where u, x and L are the displacements, position and RVE sizes, respectively (all three in vector notation). $\bar{\varepsilon}$ is the average strain tensor applied on the RVE, and t is the traction vector. It was not necessary to explicitly impose the traction boundary condition, as they were automatically satisfied by imposing the periodic displacement conditions on this periodic structure. In addition, the symmetry with respect to the $x-y$ plane was included:

$$\begin{aligned} &u_x(x,y,z) = u_x(x,y,-z), \\ &u_y(x,y,z) = u_y(x,y,-z), \\ &u_z(x,y,z) = -u_z(x,y,-z). \end{aligned}$$

The symmetry conditions were combined with the periodic conditions, and all the average shear components were set to zero. For the $x = 0$ and L_x faces this yielded the conditions:

$$\begin{cases} u_x(L_x,y,z) = u_x(0,y,z) + \bar{\varepsilon}_{xx}L_x, \\ u_y(L_x,y,z) = u_y(0,y,z) \\ u_z(L_x,y,z) = u_z(0,y,z) \end{cases} \forall (y,z),$$

for the $y = 0$ and L_y faces

$$\begin{cases} u_x(x,L_y,z) = u_x(x,0,z), \\ u_y(x,L_y,z) = u_y(x,0,z) + \bar{\varepsilon}_{yy}L_y \\ u_z(x,L_y,z) = u_z(x,0,z) \end{cases} \forall (x,z),$$

and for the $z = 0$ and $L_z/2$ faces

$$\begin{cases} u_z(x,y,0) = 0 \\ u_z(x,y,L_z/2) = \bar{\varepsilon}_{zz}L_z/2. \end{cases} \forall (x,y)$$

The tablets were modeled as transversely isotropic elastic with the moduli corresponding to those of single crystal aragonite (Hearmon, 1946; Barthelat et al., 2006a). Aragonite has an orthorhombic crystalline structure, and its [0 0 1] axis is aligned with the normal of the tablets in nacre (Sarikaya and Aksay, 1995). Its orthotropic elastic properties (nine elastic constant) were averaged in the plane of the tablets so that their modeling was reduced to transverse isotropy (five constants) with $E_P = 106\,\text{GPa}$, $E_Z = 82\,\text{GPa}$, $v_P = 0.3$, $v_{ZP} = 0.06$, $G_{ZP} = 33.45\,\text{GPa}$. P indicates the in plane direction (direction x or y) while Z indicates the out-of-plane direction.

Cohesive elements were inserted between the tablets at the interfaces and at the vertical junctions (Figs. 14 and 15). These elements have zero thickness and their behavior is

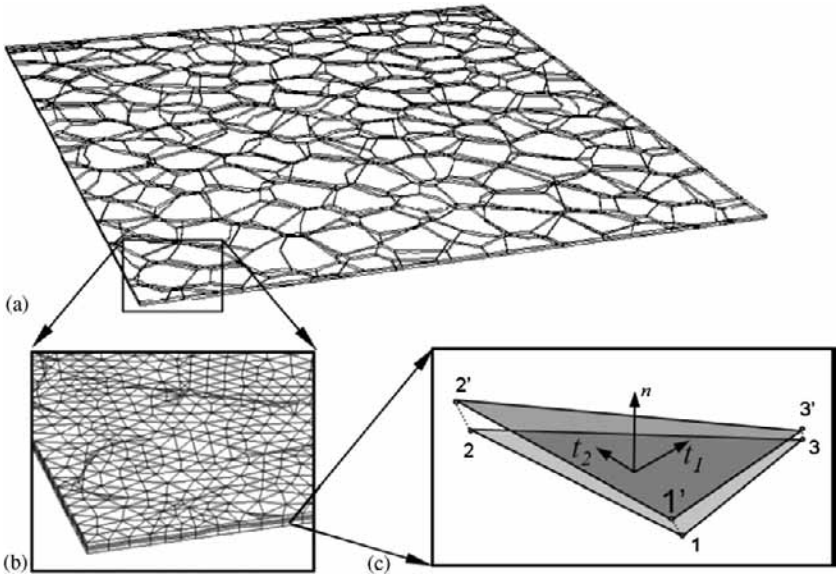

Fig. 15. (a) View of the three-dimensional model. (b) Detail of the mesh. (c) Cohesive element with local coordinate system.

formulated as a function of displacement jumps across the interface (Camacho and Ortiz, 1996; Espinosa and Zavattieri, 2003a, b). For proper cohesive elements connectivity, the tablets were meshed so their nodes were at the same coordinates (x, y) across the interface (Fig. 14b, c). Six-node cohesive elements of triangular shape were used at the interfaces, while 8-node cohesive elements of rectangular shape were used at the junctions. The mechanical parameters of the cohesive elements were assumed to identical for junctions and interfaces and they were implemented into the model using the ABAQUS user element subroutine UEL. The behavior of the cohesive elements was controlled by the effective displacement jump Δ_e, given by

$$\Delta_e = \sqrt{\Delta_{t1}^2 + \Delta_{t2}^2 + \Delta_n^2},$$

where Δ_{t1}, Δ_{t2} and Δ_n are the components of the displacement jump vector across the interface in the local tangential directions, t_1, t_2 and normal direction, n, respectively (Fig. 15).

The effective displacement controls the interface equivalent traction T_e through the cohesive law and the individual components of the traction vector are then given by

$$T_1 = \frac{\Delta_{t1}}{\Delta_e} T_e; \quad T_2 = \frac{\Delta_{t2}}{\Delta_e} T_e; \quad T_n = \frac{\Delta_n}{\Delta_e} T_e.$$

The parameters chosen for the cohesive law reflect the nanoscale mechanisms associated with mineral bridges, nanoasperities and biopolymer. As discussed in the experimental section, the first two features (bridges and asperities) cannot maintain the cohesion between tablets over long sliding distances, but they may contribute to the initial strength of the interfaces. The biopolymer, on the other hand, has significant stretching capability and can maintain cohesion between tablets over the range of tablet sliding observed

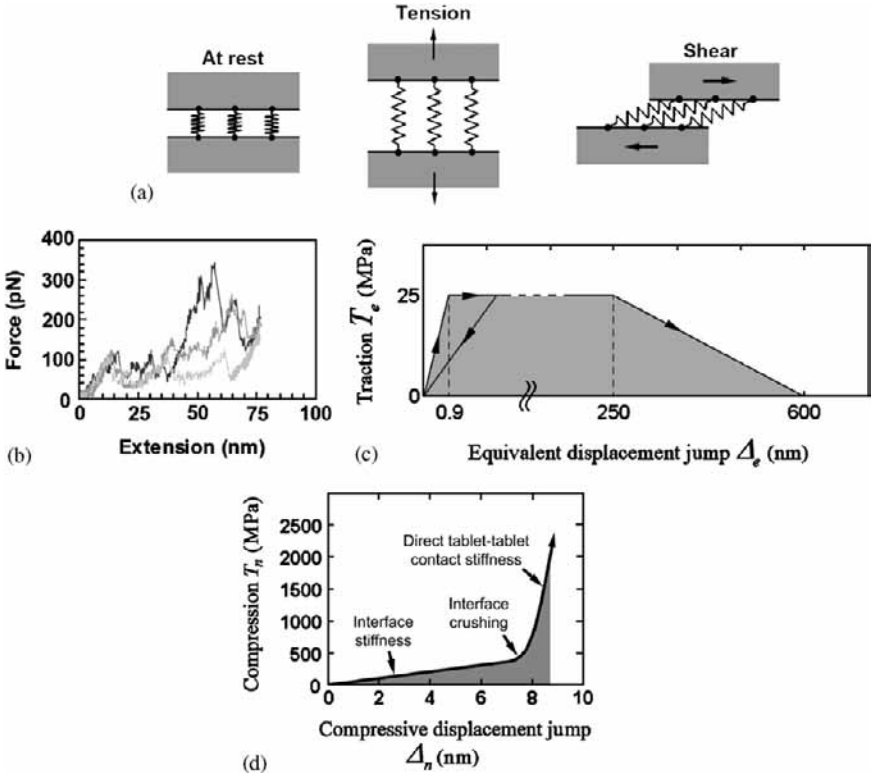

Fig. 16. (a) Idealized interface connected by springs (polymeric ligaments). Its mechanical behavior is controlled by stretching of the springs for both tensile and shear configurations. (b) Experimental results from single molecule pull (Smith et al., 1999). (c) Cohesive law: equivalent traction as function of equivalent displacement jump. (d) The compressive traction is superimposed in the case of compressive displacement jumps.

experimentally. If for large displacements the mechanics of the interface is dominated by stretching of organic ligaments, the biopolymer can be seen as a series of nonlinear spring that connect the faces of the tablets (Fig. 16a). In this simplified system, stretching of the springs (organic ligaments) controls the behavior of the cohesive element not only in tension, but also in shear. Fig. 16b shows the only experimental data available for the biopolymer at the interface, obtained by Smith et al. (1999). Note that (i) The data illustrate the large stretching capability of some of the molecules present in the interface, but might not be representative of the confined biopolymer at the interface. (ii) The organic phase is actually a very complex system in itself, composed of several layers of different polymeric species. (iii) The data does not clearly shows any significant stiffening over large strains. When a bundle of protein chains is considered, the ensemble average constitutive response is likely to exhibit an approximately constant strength over the range of displacements explored in the tensile experiment and in the present work. In the absence of further experimental data on the *nanoscale* mechanical response of the confined organic layer at the interface, it seemed reasonable to assume a constant shear strength for the cohesive law (no hardening). *This is a rather conservative assumption* and does not exclude

the possibility of polymer (interface) stiffening at larger strains. The cohesive law was set to be initially linear, followed by a long plateau and finally a linear decrease until the cohesion vanishes (Fig. 16c). Irreversible unloading was also implemented. The shear modulus of the interface was computed from the experimental shear modulus for nacre. In the simple shear experiment, the shear stress is assumed to be uniform throughout tablets and interface layers so that the Reuss composite model can be used:

$$\frac{t_I}{G_I}+\frac{t_T}{G_{ZP}}=\frac{t_I+t_T}{G_N},$$

where t_I is the interface thickness (30 nm), t_T is the tablet thickness (450 nm), G_{ZP} is the out-of-plane shear modulus of the tablets (33.4 GPa) and G_N is the shear modulus of nacre (10 GPa). Using these, the shear modulus of the interface is $G_I = 0.8$ GPa. This value was then used to compute the initial slope of the cohesive law. The shear test on nacre reported in the previous section revealed that tablet sliding starts at a shear stress of about 25 MPa. Hence, a cohesive strength of 25 MPa was used in the cohesive law. This stress level was maintained over a long plateau region. At the end of the region either the polymer stiffens and the traction stress increases, or the interface fails and the cohesive strength vanishes to zero. In this approach the second scenario was chosen. The plateau region ended at an effective displacement jump of 250 nm, which is in the order of the tablet junction openings observed on post mortem tensile specimens. From there, the strength linearly decreased with displacement, vanishing at 600 nm, which is consistent with the length of the longest observed ligament connecting two tablets (Smith et al., 1999). The simulation results actually showed that none of the interfaces totally failed within the model, the maximum sliding distance within the model being 180 nm. The chosen post-plateau behavior (either stiffening or failure) had therefore no effect on the results of the model, and neither did the choices of displacements at the onset of decohesion (250 nm) and at total failure (600 nm).

While implementing cohesive elements it is useful to determine the cohesive energy density G_C, which is the area under the traction-separation curve. Using the parameters of the present cohesive law $G_C = 10.61\,\mathrm{J/m^2}$. From this, the cohesive zone length can be computed as $l_{cz} = (9\pi E/32)(G_{Ic}/T^2_{max}) = 14\,\mu\mathrm{m}$ (Rice, 1980). The size of the associated cohesive elements should be smaller that l_{cz} in order to insure convergence (Espinosa and Zavattieri, 2003a, b), which was satisfied in the present model, the size of the cohesive elements being in the order of 0.5–1 μm.

So far in the formulation, nothing prevented the tablets from penetrating each other, which is not acceptable physically. In order to avoid tablet interpenetration, the normal component of the displacement jump was monitored at each iteration step. Negative values of Δ_n correspond to a compressed interface, and in this case the stiffness resulting from contact should be much higher than the stiffness of the interface in tension or shear. In such event, a compressive traction, function of compressive normal displacement jumps (Fig. 16d), was superimposed on the elements. The initial compressive stiffness was computed based on the thickness of the interface (30 nm) and the compressive modulus of the interface, 2.8 GPa measured experimentally from an uniaxial compression test across the tablets (Barthelat et al., 2006a). Upon reaching compressions of about 400 MPa, the interface is crushed (Barthelat et al., 2006a) and the compressive behavior is controlled by direct tablet–tablet contact. The resulting compressive stiffness was therefore chosen based on the out-of-plane modulus of aragonite (82 GPa). In the simulations, the compressive stresses actually never reached the point where the crushing stresses for the interfaces.

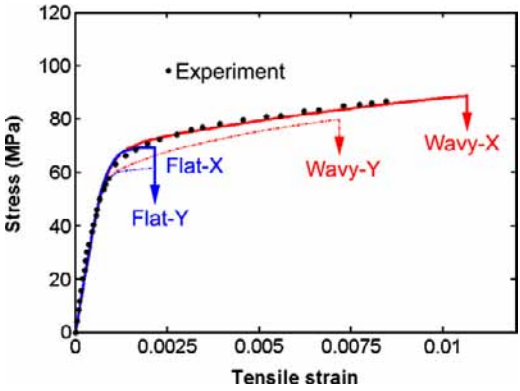

Fig. 17. Stress–strain curves as predicted by the wavy and flat models stretched along the x and y directions.

7. Simulations results

Because of limitations in the cohesive law formulations, simple shear simulation could not be performed accurately using this RVE model. Out-of-plane tablet separation in simple shear is much greater that in tension, and the mechanical response of the highly distorted interfaces during the shear test could not be captured with the present cohesive law. On the other end interface deformations due to tensile strains on the RVE are smaller and were successfully modeled. Average tensile strains of increasing magnitude were prescribed on the 3D RVE, and stretching along both x and y directions were considered. Fig. 17 shows the stress–strain curves predicted by the flat (flat interface) and wavy (wavy interface) models. All simulations predicted the same elastic behaviors, with a modulus consistent with the experiments on hydrated nacre. As expected, the modeled RVE provides almost identical responses when the material was stretched in the x or y direction. This shows that enough tablets were included in the RVE to capture the statistics of the microstructure. Including more tablets in the RVE would probably bring the behavior along the x and y axes closer to each other (at an increased computational expense), but would not change the main conclusions of the simulation. Wavy and flat models showed similar initial strengths, but as the deformation increased the wavy model showed more hardening than the flat model. The flat model ceased to converge at a strain of 0.004 while the wavy model ran up to a strain of 0.008–0.01 (for a maximum tablet separation of 180 nm). Since the calculations were quasi-static, lack of convergence was ascribed to the development of an instability (or to an onset of catastrophic/unstable crack propagation along the interface) and to a change in the character of the governing equations.

Fig. 18 shows a plot of the displacement contours along the loading direction (x axis) for both flat and wavy models, at an average strain $\bar{\varepsilon}_{xx} = 0.004$. The flat model shows a clear localization of deformation on the right-hand side of the model. The variation of u_x along x shows that the localization appeared early in the deformation of the RVE ($\bar{\varepsilon}_{xx} = 0.002$). From this point, the model could not be assumed to be representative of the volume anymore, since by definition a localization appears at only one location in the material.

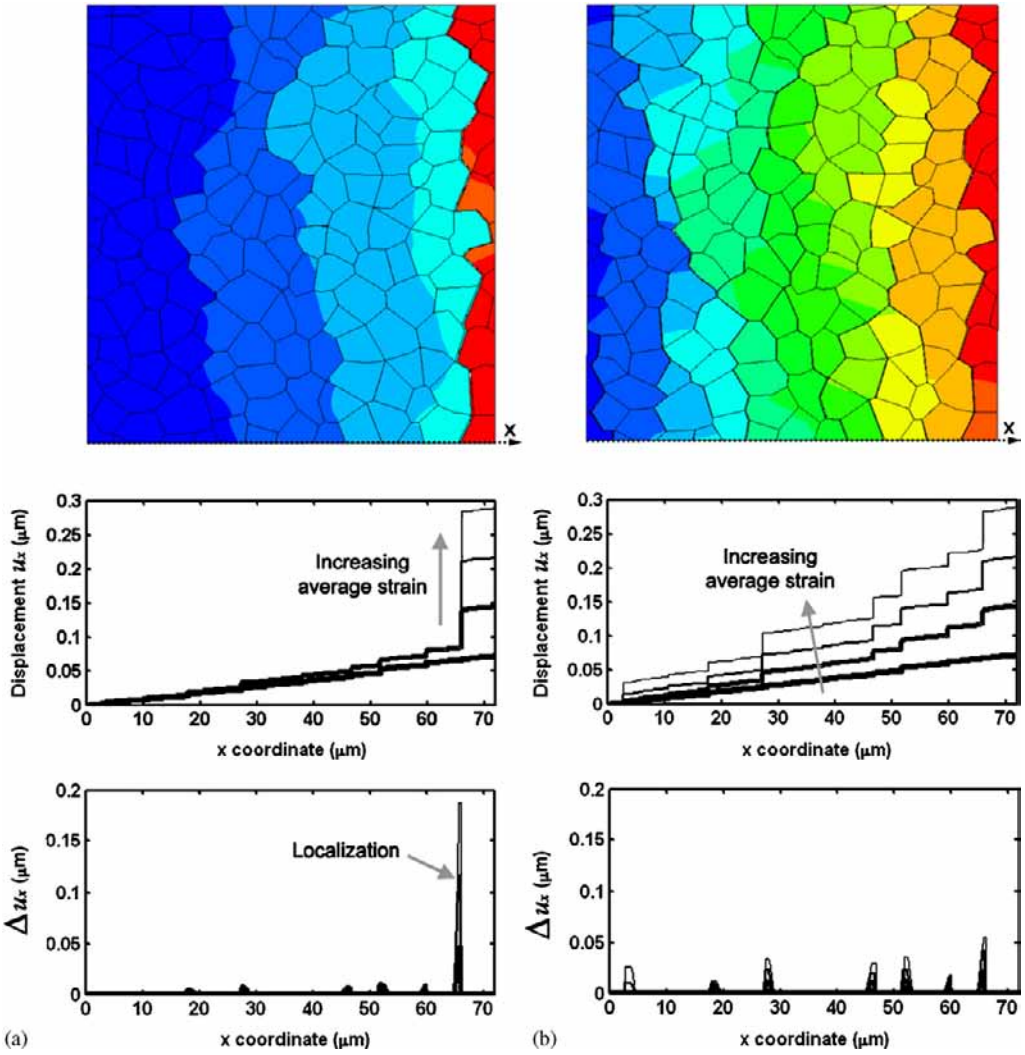

Fig. 18. u_x displacement contours, u_x path plot along the x axis (dotted line) and displacement jump Δu_x across the interface for increasing average strains (0.001, 0.002, 0.003 and 0.004): (a) model with flat tablets: the deformation localizes early on the right side of the model; (b) model with wavy tablets, showing a more uniform deformation.

It is more physical to assume that the volumes of materials on the left and on the right-hand sides of the RVE are still intact, in which case the material fails at the macroscale as soon as the localization appears (as shown on the stress–strain curve of Fig. 17). By contrast to the flat case, the wavy model shows a uniform distribution of deformation throughout the RVE for all the explored strain levels. Tablet sliding takes place in the overlap regions of the RVE, in agreement with the experimental observations. Fig. 18b shows that the magnitude of u_x along x (at $y = 0$) progressively increases with small steps every 5–10 μm, corresponding to the formation of voids at the sliding sites, spaced by one

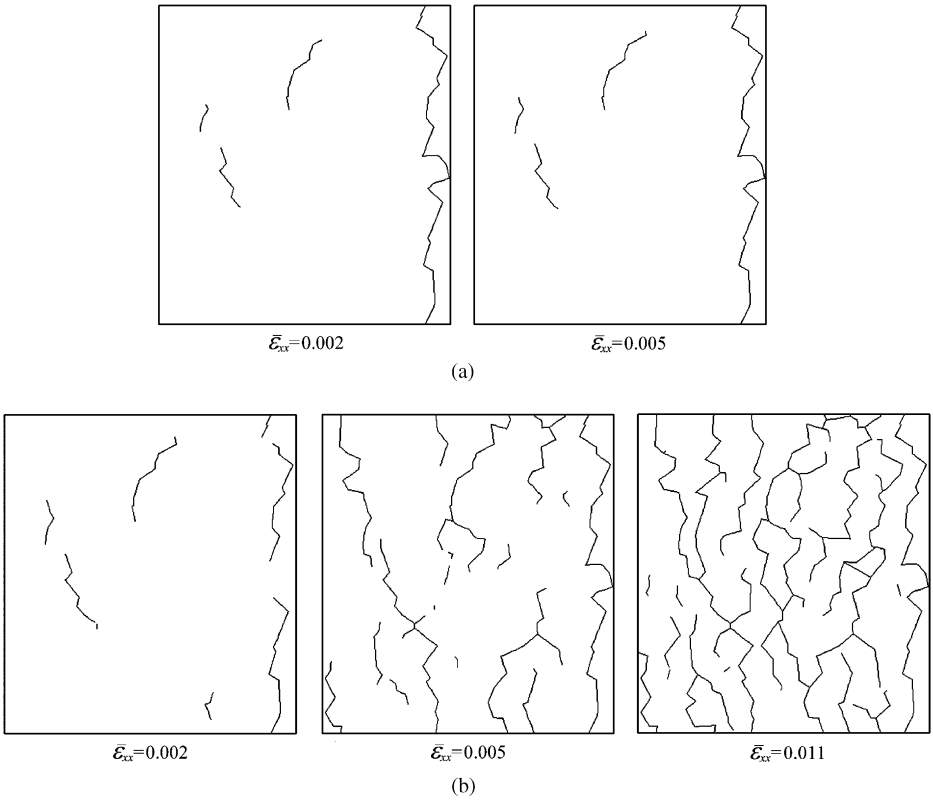

Fig. 19. Top cohesive junction elements for which the equivalent displacement jump is greater than 20 nm, plotted at different average strain levels: (a) flat case, showing early localization. Note that the model ceased to converge beyond $\bar{\varepsilon}_{xx} = 0.05$; and (b) wavy case, showing distribution of deformations.

tablet diameter. Fig. 19 shows a "crack pattern" plot for the flat and wavy models. The flat model localizes deformation early. Note that the wavy model shows the same pattern initially, but it is able to spread deformation for larger strains. Prior to instability and failure, most of the potential sliding sites are activated. Fig. 20a and b show the displacement jumps along the x direction for the wavy and flat cases, respectively. Again, the localization is clearly visible for the flat case. The openings of the vertical junction elements follow the same patterns as the interface elements, as shown on Fig. 20c. These simulation results show that while a material capable of maintaining cohesion over large displacements is necessary at the interface, it is not sufficient to provide the required hardening. Even in the absence of hardening at the nanoscale, the hardening rate observed experimentally for nacre could be matched via mechanisms associated with microscopic tablet waviness. Under tensile loading, the hardening allows relatively large strains to develop and propagate over large volumes. This is a clear departure from the typical mechanical behavior of a ceramic. Fig. 20d shows a cross section of the wavy model, revealing a specific where two tablets were progressively locked by their waviness. This specific type of morphologies, discussed in the next section, generate the locking mechanism in the wavy model.

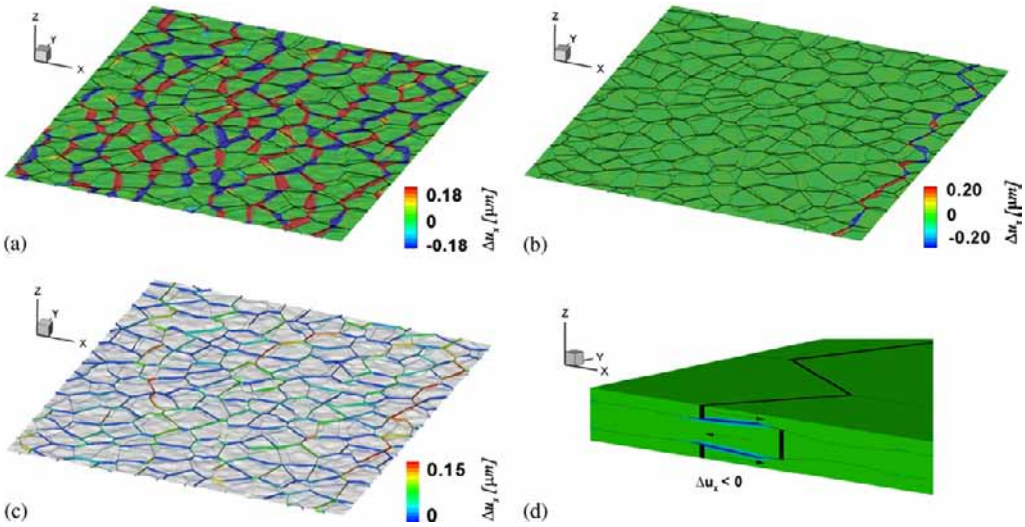

Fig. 20. (a) Displacement jump Δu_x across the interfaces, wavy case ($\bar{\varepsilon}_{xx} = 0.011$). (b) displacement jump Δu_x across the interfaces, flat case ($\bar{\varepsilon}_{xx} = 0.005$). Note the localization. (c) Displacement jump Δu_x across the junction elements, wavy case ($\bar{\varepsilon}_{xx} = 0.011$). (d) Detail of the cross section of the wavy model, showing a dovetail (the symmetry with respect to the $x-y$ plane as been applied for this display).

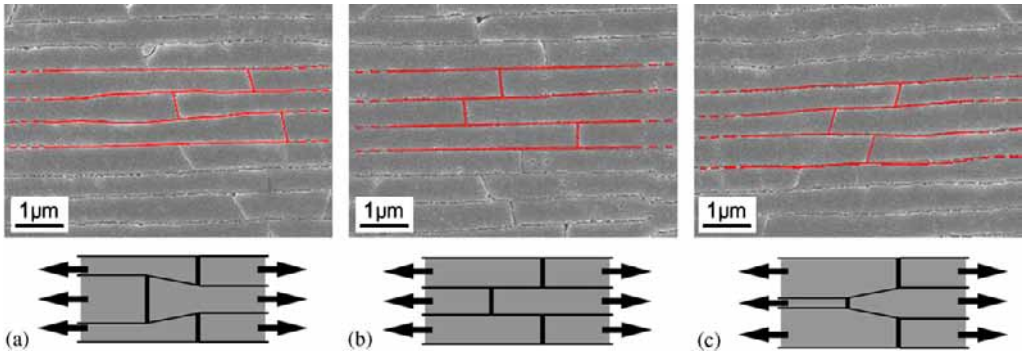

Fig. 21. Scanning electron micrographs and schematics of tablet geometries in overlap regions: (a) dovetail; (b) flat; (c) "inverse" dovetail.

8. Hardening features

The specific hardening features that generate the distribution of deformations and large strains at failure will now be examined. As observed in the experiments and simulations, sliding of the tablets on one another occurs in the overlap regions. Obstacles to tablet sliding must therefore be located in these areas. Scanning electron micrographs of polished nacre show that in some locations, the waviness of the interface generates tablets that are thicker at their periphery (Fig. 21a). In two dimensions the shape is very similar to a dovetail, a locking device widely used in mechanical assembly. As opposed to traditional dovetails however, the angle are not so high that the locking is total, but the geometry is

such that progressive pullout, accompanied by hardening, is allowed. Many of these "dovetails" were observed in two-dimensional cross sections of nacre. In about equal proportion, the overlap regions appeared to be flat (Fig. 21b). Finally, in rare occurrences, the tablet actually becomes thinner into the overlap region. (Fig. 21c). The last case is clearly the weakest connection, since the normal traction on the surface probably precipitates the failure of the interfaces.

The finite element RVE employed in the simulations contained such features as a natural outcome of incorporating a large number of tablets with measured tablet waviness. In this section the dovetail feature is examined in more detail, since such features are the source of the macroscopic strain hardening. Fig. 22 shows a cross section of the RVE showing a tablet overlap area with "dovetail" geometry loaded in tension (the section was mirrored about the $z = 0$ line for clarity). The stress contours correspond to the last deformation step (immediately prior to failure) of the tensile stretching along the x direction. The black area at the junction corresponds to the void generated by tablet separation. As expected, the stress contours are consistent with load transfer through interface shear in the overlap region (Fig. 22a–c). In this process, stress concentrations are generated within the tablets, near the junctions, with a maximum of 300 MPa in the section showed (it reached 550 MPa

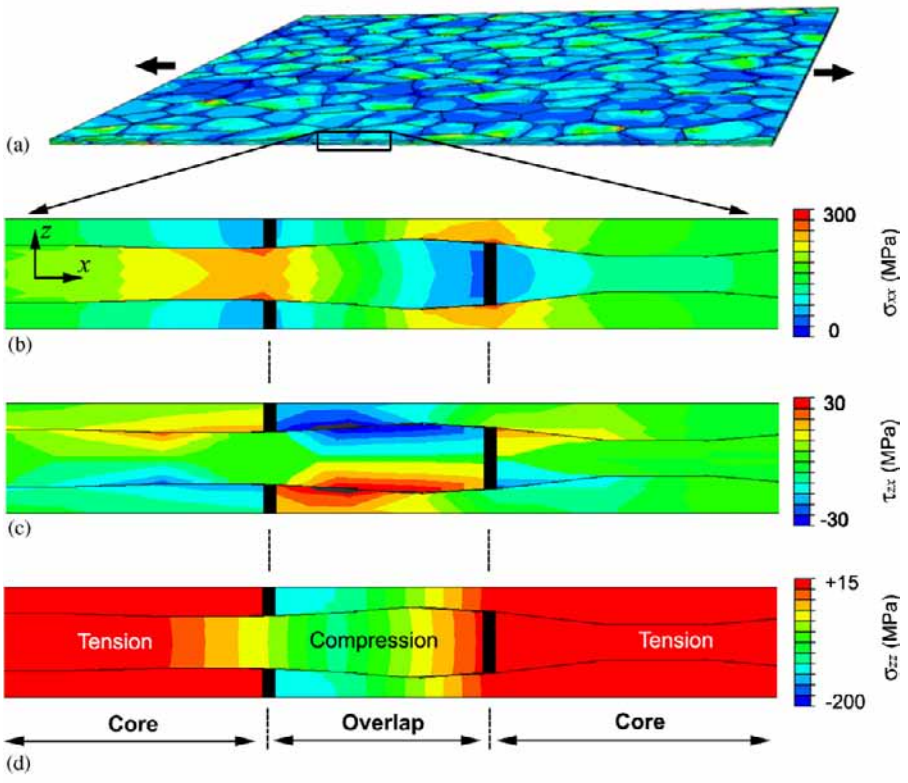

Fig. 22. (a) Tensile stresses σ_{xx} in the entire RVE. (b) Tensile stresses σ_{xx} in a small cross section of the RVE. (c) Shear stresses, showing concentrations near the interfaces. (d) Out-of-plane stress σ_{zz} showing compression in the overlap region and tension in the core region. Stress contours in a cross section of the model.

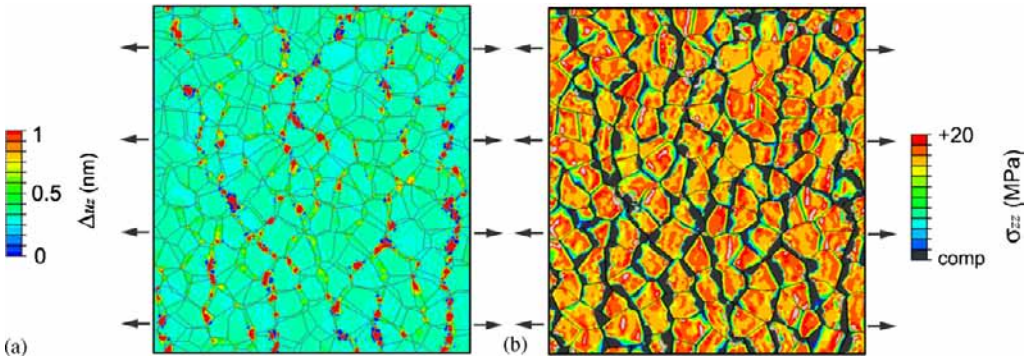

Fig. 23. (a) Displacement jump Δu_z across the interface elements for the wavy model; (b) out-of-plane stresses. The darker regions are in compression and are an indication of locking (contours taken for the last deformation step prior to failure).

in other locations within the RVE). These are relatively high stresses that emphasize the importance of strong tablets. In this respect, it was shown that their small size confers them with superior strength (Gao et al., 2003), and the presence of nanograins may also be beneficial (Li et al., 2004). Nevertheless, tablet fracture is an event that cannot be totally ruled out, and a small fraction of the tablets may fail in tension during a tensile test (Currey, 1977). Fig. 22d shows the stress distribution in the out-of-plane direction. As a result of progressive tablet locking a significant compression develops in the overlap area (−200 MPa). In order to maintain equilibrium (for a uniaxial tension test along x or y, $\bar{\sigma}_{zz} = 0$ over the entire RVE), a region of transverse tensile stresses develops in the core area. The level of tensile stress is between 10 and 15 MPa in the considered cross-section, which is below the tensile strength of the interface (25 MPa). In order for locking to take place, the interface in the core region has to withstand such tensile stresses. Should they reach the strength of the interface (25 MPa) in the core of the tablets, the interface would fail, the tablets would split and the locking stresses would vanish. This might be a possible failure mechanism for nacre in tension. At this point, it is interesting to note that the mineral bridges seem to be concentrated in the center of the tablets (Song et al., 2002), and while they do not affect the interface in the sliding regions, they might strengthen the core areas and prevent the delamination of the tablets.

The simulations show that the dovetail geometry of the tablet is a powerful hardening feature. However not all overlap regions benefit from such locking mechanism. As mentioned above, there is an equal number of completely flat overlap and a few occurrence of "inverted" dovetails. The extent of locking can be tracked by monitoring the displacement jump along the z direction across the interface elements, and the out-of-plane stresses. Fig. 23a shows that the interface separate along the z direction, in overlap regions where locking operates. Significant out-of-plane compressive stresses develop in the same regions, as shown in Fig. 23b. Dark regions are regions of compressive stress and tablet locking, while the rest of the RVE is under tensile stress. About 15% of the volume of the model experiences transverse compression, the rest being in tension. Recalling that the tablet overlap areas compose about 30% of the area of a layer, this shows that half of the overlap areas are interlocked. Although progressive tablet locking does not

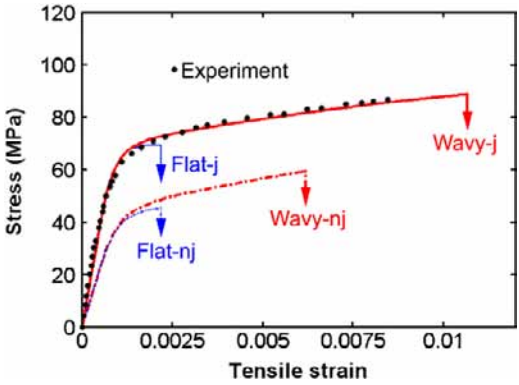

Fig. 24. Tensile stress–strain curves for models with junctions (flat-*j* and wavy-*j*) and without junctions (flat-*nj* and wavy-*nj*).

happen everywhere in the model, it is sufficiently strong to shield the weakest areas from excessive stresses and to generate hardening at the macroscale.

9. Effect of the tablet junctions

The RVE model under examination lends itself to examine the effects of the tablet junctions. To this end, two cases were compared. The original case was considered above and has cohesive elements at both interfaces and junctions, while the second case was based the same model, but the cohesive elements at the junctions were removed. Both flat and wavy cases were considered, and both models were stretched along the x direction. The results are shown in Fig. 24. In the elastic region, the junctions add to the stiffness of the RVE: removing the junctions lowers the modulus from 70 to 40 GPa. The strength drops from 70 MPa with junctions to 45 MPa without junctions, which can be explained as follows: as tablets separate, the maximum tensile stress across the junctions is rapidly reached, and from then on the junctions provide a constant additional tensile stress equal to their strength (25 MPa). While the junctions add stiffness and strength to the RVE, they do not seem to affect the hardening rate.

10. Perfectly hexagonal tablets

Until this point, a RVE model with statistical distributions of tablet size and arrangement was used. In this section, a RVE model composed of perfectly hexagonal tablets is considered. Such model is devoid of statistics, as all the tablets have the same size and overlap. Such periodic geometry could have been modeled using a smaller RVE of the size of the tablet, but in the present case many tablets were again included in order to capture possible localization of deformation. Such arrangement is relevant in the context of fabricating synthetic composites that mimic nacre; hence, it is useful to assess its performance and to compare to the real structure of nacre. The size of the hexagonal tablets was based on the average area measured on the actual microstructure (35 μm^2), and their thickness was the same as in the real material. The overlap was introduced by shifting

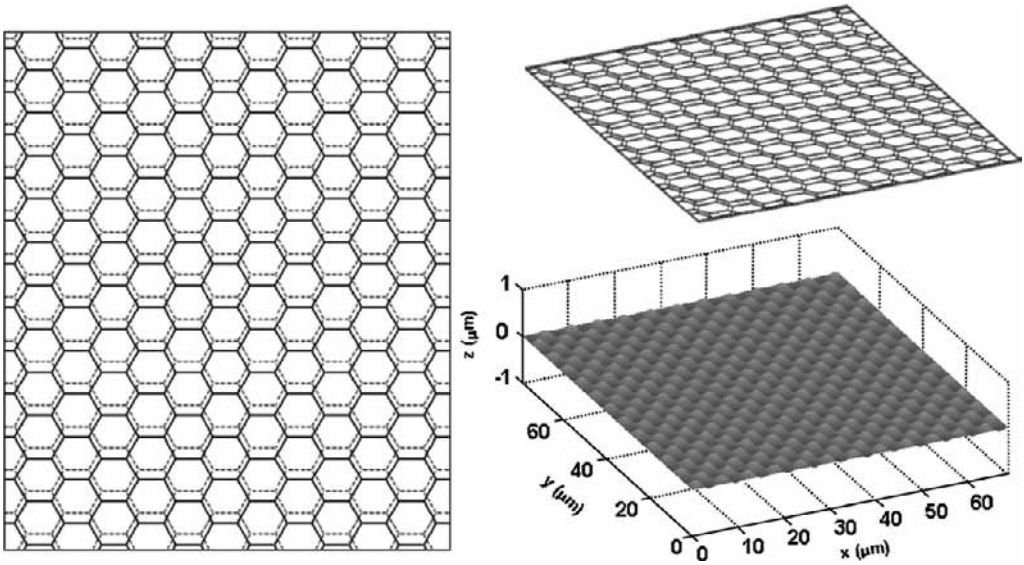

Fig. 25. Tablet arrangement for the hexagonal tablet model.

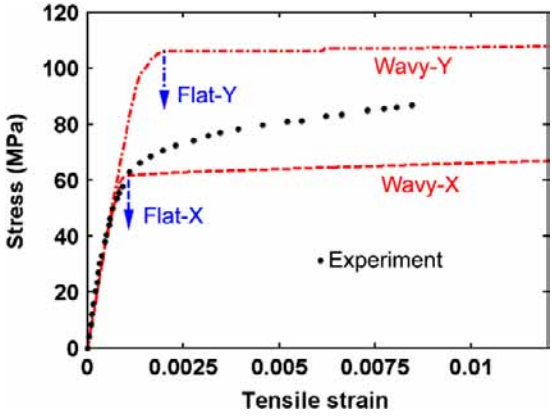

Fig. 26. Stress–strain curve for perfect hexagon models stretched along x and y directions.

the tablets of the top layer along the y direction. The amount of shifting was set to 1.56 μm, so that the overlap area covered 30% of the surface area of the layer, like in the real material. The waviness was modeled as a sinusoidal surface with characteristics based on the actual waviness; i.e, amplitude of 100 nm and a wavelength of 5 μm. The cohesive law was the same as the one employed for the real model. This model therefore retains the features of the real microstructure, but it is devoid of any statistics (Fig. 25). Fig. 26 shows the stress–strain curves predicted by the simulations. The model reproduces the experimental modulus in both x and y directions. However, the strengths are very

different in the x (60 MPa) and y (105 MPa) directions. This is due to the overlap area involved in the load transmission by shear, which is much smaller when the model is stretched along the x direction as compared to when the model is stretched along the y direction. As one can envision, the transition from elasticity to tablet sliding for the hexagonal tablet model is more abrupt than that for the real case because of the absence of statistics. The sinusoidal surface generates hardening and large deformation like the real waviness does, but to a smaller rate. Interestingly, the hexagonal model seemed to achieve larger deformations prior to sliding saturation, and in fact the calculations were stable to strains up to 0.03. The hardening rate, however, was much lower than for the case with real microstructure. For the cases with flat tablets, the strains at failure were greater for the model with real contour than for the models with hexagonal contour. Statistics in the microstructure, although less important than the waviness of the tablet, therefore plays a role in the strengthening of nacre. This emphasizes the importance of incorporating some randomness in the microstructural design of artificial materials mimicking nacre.

11. Conclusions

Tensile, shear and shear-compression tests were performed on dry and hydrated miniature nacre specimens. The experiments revealed that nacre exhibits inelastic strains in tension (up to 1% strain at failure) when hydrated. Simple shear tests and shear-compression tests also demonstrated the large inelastic deformations and strain hardening of nacre under hydrated conditions. Dry specimens possess higher strength but are more brittle. Normal compressive stresses across the interfaces have a limited effect on the shearing resistance of hydrated nacre, but they significantly increase the shear strength of dry nacre. All tests showed that shearing of the layers is accompanied by a significant lateral expansion, suggesting some type of climbing mechanism.

A finite element model of a three-dimensional representative volume element of hydrated nacre was implemented and analyzed. The simulations revealed that even when the interface does not harden at the nanoscale, the waviness of the tablets could generate the strain hardening observed experimentally. Such feature distributes the inelastic deformation and stabilizes the material up to relatively large strains. Specific overlap geometries were identified, with dovetails-like features acting as powerful locking mechanisms. These features are not present everywhere in the microstructure, but in sufficient number to generate macroscale hardening and to shield the weaker areas from excessive stresses. The tablet junctions provide additional strength to the microstructure, but do not generate any additional hardening nor stabilize the material response. RVE models made of perfectly hexagonal tablets and perfect waviness showed a significant anisotropy and lower hardening rate.

In the past, several explanations have been advanced to interpret the mechanical behavior of nacre. Some of the most prominent ones are summarized and discussed here:

- Nanoasperities on the surface of the tablets were proposed as a source of resistance to tablet sliding (Evans et al., 2001; Wang et al., 2001). However, the models presented showed these features could provide resistance over sliding distances of only 15–20 nm, much smaller than the 100–200 nm observed experimentally. In addition, TEM images such as Fig. 3a show that the interaction between asperities of opposed tablets is actually relatively limited.

- Nanograins within the tablets were proposed as tablet strengthening features (Li et al., 2004). Clearly, this may be beneficial to the overall performance of nacre. However, the tablet strength does not directly affect the main deformation mechanism in nacre, which is tablet sliding. Its relevance is linked to the preservation of tablet integrity in the deformation process.
- The stretching capabilities of some of the biomolecular species within the interface of the tablets is certainly of importance for the toughness of nacre (Smith et al., 1999). However, the strain hardening of the biopolymer is limited and is not sufficient to explain the macroscopic strain hardening of nacre.

While the above features are beneficial to the behavior of nacre, they are not *sufficient* to explain its mechanical performance. In the present work we showed that tablet waviness appears as a critical microstructural feature responsible for its relatively large inelastic deformations and its strength. Even with a non-hardening cohesive law, tablet waviness generates progressive tablet interlocking during tablet sliding and the propagation of inelastic deformations over large volumes. Such behavior has certainly some impact on the fracture toughness of nacre. The formation of a large region of inelastically deformed material around cracks and defects is believed to be an important toughening mechanism for nacre, comparable to transformation toughening (McMeeking and Evans 1982; Wang et al., 2001). Inelastic deformations also impart materials with damage tolerance, reducing stress concentrations around defects (McNulty et al., 1999; Evans et al., 2001). The mechanics of tablet sliding and inelastic deformation was actually correlated to the toughness of nacre, through a process zone type model (Barthelat et al., 2006b).

From the identified hierarchical structure of nacre, the mechanical testing and the numerical simulations, some design guidelines for synthetic composites that mimic nacre can be envisioned and are summarized here:

- The material of the tablets should be stiff and have a high tensile strength. To achieve high strength small tablet size should be employed. Tablet materials with nanograins inclusions can also be used as they may increase strength.
- The interface between the tablets should be made of a much softer material capable of withstanding large strains. No strain hardening is required for this material.
- The interface should have a high compressive stiffness and high compressive strength in the out-of-plane direction in order for the progressive locking mechanisms to operate. Since the material at the interface needs to be relatively soft, this requirement implies that the interface must be as thin as possible to increase stiffness. Thin interfaces also promote confinement and compressive strength.
- The shape of the tablets should be of high aspect ratio to maximize the overlap areas and the load transmitted from one column of tablets to the next, by interface shearing. However the thickness should be optimized to avoid tablet failure before tablet sliding.
- The arrangement of the tablets within each layer should resemble a Voronoi tiling with some degree of randomness to provide overlap and to insure in-plane isotropy.
- The interface between the tablets should be wavy to generate the locking devices required for hardening.
- Core area, interface tensile strength and waviness amplitude should be finely tuned. In order for the locking to operate, the interfaces in the core area must withstand transverse tensile stresses to balance the climbing force arising from the transverse

compression in the locking region. In this context, it is worth noting that nanoscale mineral bridges, concentrated at the center of the tablets (Song and Bai, 2002), may provide the required tensile strengthening of the interface in the core regions.

In closing, we would like to highlight that all these observations could in principle be mathematically formulated within an optimization scheme. Clearly, the highly non-linear nature of the governing equations and the synergy between geometry and mechanical features make the problem quite complex. Nacre is an example of a powerful solution to the problem, resulting from millions of years of evolution. It remains to be demonstrated that manmade materials can achieve such degree of sophistication and performance for a given set of objectives and constraints.

Acknowledgements

This work was supported by the National Science Foundation through award No. CMS-0301416. We would like to thank Dr. Ken Chong for his encouragement and support during this investigation. We would also like to thank Dr. Kevin Cummings for his donation of freshwater mussel specimens.

References

Barthelat, F., Li, C.M., et al., 2006a. Mechanical properties of nacre constituents and their impact on mechanical performance. J. Mater. Res. 21 (8), 1977–1986.

Barthelat, F., Tang, H., et al., 2006b. On the microscopic origins of the toughness of nacre, submitted.

Blank, S., Arnoldi, M., et al., 2003. The nacre protein perlucin nucleates growth of calcium carbonate crystals. J. Mic.—Oxford 212, 280–291.

Bruet, B.J.F., Qi, H.J., et al., 2005. Nanoscale morphology and indentation of individual nacre tablets from the gastropod mollusc Trochus niloticus. J. Mater. Res. 20 (9), 2400–2419.

Camacho, G.T., Ortiz, M., 1996. Computational modelling of impact damage in brittle materials. Int. J. Solids Struct. 33 (20–22), 2899–2938.

Currey, J.D., 1977. Mechanical properties of mother of pearl in tension. Proc. R. Soc. London 196 (1125), 443–463.

Currey, J.D., Taylor, J.D., 1974. The mechanical behavior of some molluscan hard tissues. J. Zool. (London) 173 (3), 395–406.

Espinosa, H.D., Zavattieri, P.D., 2003a. A grain level model for the study of failure initiation and evolution in polycrystalline brittle materials. Part I: Theory and numerical implementation. Mech. Mater. 35 (3–6), 333–364.

Espinosa, H.D., Zavattieri, P.D., 2003b. A grain level model for the study of failure initiation and evolution in polycrystalline brittle materials. Part II: numerical examples. Mech. Mater. 35 (3–6), 365–394.

Evans, A.G., Suo, Z., et al., 2001. A model for the robust mechanical behavior of nacre. J. Mater. Res. 16, 2475–2484.

Feng, Q.L., Cui, F.Z., et al., 2000. Crystal orientation, toughening mechanisms and a mimic of nacre. Mater. Sci. Eng. C–Biomimet. Supramol. Systems 11 (1), 19–25.

Gao, H.J., Ji, B.H., et al., 2003. Materials become insensitive to flaws at nanoscale: lessons from nature. Proc. Natl. Acad. Sci. USA 100 (10), 5597–5600.

Hearmon, R.F.S., 1946. The elastic constants of anisotropic materials. Rev. Mod. Phys. 18, 409–440.

Jackson, A.P., Vincent, J.F.V., et al., 1988. The mechanical design of nacre. Proc. R. Soc. London 234 (1277), 415–440.

Ji, B.H., Gao, H.J., 2004. Mechanical properties of nanostructure of biological materials. J. Mech. Phys. Solids 52 (9), 1963–1990.

Katti, D.R., Katti, K.S., 2001. Modeling microarchitecture and mechanical behavior of nacre using 3D finite element techniques. Part 1. Elastic properties. J. Mater. Sci. 36, 1411–1417.

Katti, D.R., Pradhan, S.M., et al., 2004. Modeling the organic–inorganic interfacial nanoasperities in a model bio-nanocomposite, nacre. Rev. Adv. Mater. Sci. 6 (2), 162–168.
Katti, K.S., Katti, D.R., et al., 2005. Platelet interlocks are the key to toughness and strength in nacre. J. Mater. Res. 20 (5), 1097–1100.
Kotha, S.P., Li, Y., et al., 2001. Micromechanical model of nacre tested in tension. J. Mater. Sci. 36 (8), 2001–2007.
Li, X.D., Chang, W.C., et al., 2004. Nanoscale structural and mechanical characterization of a natural nanocomposite material: the shell of red abalone. Nano Lett. 4 (4), 613–617.
Manne, S., Zaremba, C.M., et al., 1994. Atomic-force microscopy of the nacreous layer in mollusk shells. P. Roy. Soc. Lond. B. Bio. 256 (1345), 17–23.
Mayer, G., 2005. Rigid biological systems as models for synthetic composites. Science 310 (5751), 1144–1147.
McMeeking, R.M., Evans, A.G., 1982. Mechanics of transformation-toughening in brittle materials. J. Am. Ceram. Soc. 65 (5), 242–246.
McNulty, J.C., Zok, F.W., et al., 1999. Notch-sensitivity of fiber-reinforced ceramic-matrix composites: effects of inelastic straining and volume-dependent strength. J. Am. Ceram. Soc. 82 (5), 1217–1228.
Menig, R., Meyers, M.H., et al., 2000. Quasi-static and dynamic mechanical response of haliotis rufescens (abalone) shells. Acta Mater. 48.
Okumura, K., de Gennes, P.G., 2001. Why is nacre strong? Elastic theory and fracture mechanics for biocomposites with stratified structures. Eur. Phys. J. E 4 (1), 121–127.
Peters, W.H., Ranson, W.F., 1982. Digital imaging techniques in experimental stress-analysis. Opt. Eng. 21 (3), 427–431.
Rice, J.R., 1980. The Mechanics of Earthquake Rupture. Italian Physical Society, North-Holland Publ. Co., Italy, Amsterdam.
Sarikaya, M., Aksay, I.A. (Eds.), 1995. Biomimetics, Design and Processing of Materials. Polymers and Complex Materials. Woodbury, New York.
Schaeffer, T.E., IonescuZanetti, C., et al., 1997. Does abalone nacre form by heteroepitaxial nucleation or by growth through mineral bridges? Chem. Mater. 9 (8), 1731–1740.
Smith, B.L., Schaeffer, T.E., et al., 1999. Molecular mechanistic origin of the toughness of natural adhesives, fibres and composites. Nature (London) 399 (6738), 761–763.
Song, F., Bai, Y., 2002. Nanostructure of nacre and its mechanical effects. Int. J. Nonlinear Sci. Numer. Simul. 3.
Song, F., Bai, Y.L., 2003. Effects of nanostructures on the fracture strength of the interfaces in nacre. J. Mater. Res. 18, 1741–1744.
Song, F., Zhang, X.H., et al., 2002. Microstructure in a biointerface. J. Mater. Sci. Lett. 21, 639–641.
Wang, R.Z., Wen, H.B., et al., 1995. Observations of damage morphologies in nacre during deformation and fracture. J. Mater. Sci. Lett. 30 (9), 2299–2304.
Wang, R.Z., Suo, Z., et al., 2001. Deformation mechanisms in nacre. J. Mater. Res. 16, 2485–2493.